Theory of photorefractive vectorial wave coupling in cubic crystals

B. I. Sturman and E. V. Podivilov
International Institute for Nonlinear Studies, Siberian Branch, Koptyg Prospect 1, 630090 Novosibirsk, Russia

K. H. Ringhofer, E. Shamonina, and V. P. Kamenov
Physics Department of the University, D-49069 Osnabrück, Germany

E. Nippolainen, V. V. Prokofiev, and A. A. Kamshilin
Department of Physics of the University, P.O. Box 111, Joensuu, Finland
(Received 26 January 1999)

We present an analytical theory of vectorial wave coupling in photorefractive cubic crystals which are, in general, optically active. The theory is based on the systematic use of the spatial symmetry properties and the apparatus of the Pauli operators to deal with two-dimensional vectors and matrices. It allows one to give a unified description of a wide spectrum of photorefractive phenomena, including the efficiency and polarization properties of Bragg diffraction, polarization two-beam coupling enhanced by ac fields, the influence of the photoelastic effect, etc. Applications of the theory to crystals of the sillenite family and to particular photorefractive phenomena are given. A good qualitative agreement between the theoretical predictions and experimental data for $Bi_{12}TiO_{20}$ (BTO) crystals is shown. [S1063-651X(99)12209-8]

PACS number(s): 42.70.Nq, 42.65.Hw

I. INTRODUCTION

Photorefractive nonlinear wave coupling has been the subject of many studies [1–3]. Usually the strongest photorefractive optical nonlinearity and, correspondingly, the strongest wave interactions occur in photorefractive ferroelectrics, which are highly anisotropic. The wave surfaces for two light eigenmodes (often ordinary and extraordinary waves) are well separated here in $\vec{k}$ space. For this reason, wave interactions in ferroelectrics may succesfully be described by coupled equations for the scalar wave amplitudes. The polarization properties of the wave coupling are uncoupled here from the effects of energy and phase exchange.

Unfortunately, the photorefractive response of ferroelectrics is not sufficiently fast for optical applications. Much effort has been made to find faster photorefractive materials [1–3]. Nowadays, cubic crystals of the sillenite family [$Bi_{12}SiO_{20}$ (BSO), $Bi_{12}TiO_{20}$ (BTO), and $Bi_{12}GeO_{20}$ (BGO)] meet the necessary requirements most fully. In the absence of applied electric fields these materials are optically isotropic and optically active.

Two techniques (dc and ac) have been proposed to enhance the value of the photorefractive response in sillenites [4,5]. Both of them exploit applied electric fields. In the dc case this field is constant and the interacting light waves are slightly shifted in frequency from each other. In the ac case, which is proven to be most useful, an applied field oscillates in time and no frequency shift is needed between the light waves. The efficiency of the ac technique depends on the temporal profile of the applied field [6]. The best enhancement corresponds to a square-wave profile when the ac field changes its sign periodically.

Considerable progress in improving the photorefractive characteristics of sillenites has been made several years ago [7,8]. The fabrication of thin and long (fiberlike) BSO and BTO crystals has allowed an increase in the amplitude of the ac field up to 50 kV/cm, a decrease in the response time in cw experiments to microseconds, and a demonstration of a variety of strong nonlinear effects relevant to applications, such as fast phase conjugation [9], generation of surface light waves [10,11], and time separated recording and readout processes [12].

The main problem and the main specific features in describing the photorefractive wave coupling in cubic crystals is the vectorial character of the interaction. The distance between the wave surfaces in $\vec{k}$ space that corresponds to two eigenwaves (elliptically polarized in the presence of an applied electric field) is considerably smaller here than in ferroelectrics. For this reason, the energy and polarization exchange between light waves cannot generally be held apart and, correspondingly, the vectorial wave coupling cannot be reduced to the scalar one. The proximity of the wave surfaces, together with the specific features of the electro-optic effect in cubic crystals, also means that the wave coupling is highly sensitive to the input wave polarizations, to the crystal cut, to the applied field, etc. A wealth of strong nonlinear phenomena, a high spatial symmetry, and an apparent simplicity of formulation of the nonlinear problems is a challenge for theorists in the field of photorefraction.

The theoretical description of the photorefractive nonlinear phenomena in cubic crystals, in general, and in the sillenites, in particular, remains, is spite of a great number of publications, very fragmental; at present it does not meet the requirements for experiment. The essence of the theoretical studies performed may be sketched as follows.

A considerable number of papers has been devoted to the analysis of vectorial wave coupling via a spatially uniform grating of the space-charge field [12–17]. The results obtained have shown the importance of the polarization degree of freedom and the orientation of the grating fringes about the crystal axes for optimization of the readout process. Many of the above papers use various approximations or numerical methods to solve the vectorial Bragg-diffraction

 © 1999 The American Physical Society

problem. It has become clear only recently [16,17] that this problem can be solved exactly in the paraxial limit. In any event, the assumption of a uniform grating cannot be applied to the cases of strong energy and polarization exchange between the interacting light beams.

The effects of weak two-wave (2W) coupling have been considered in Refs. [18–20] using the approximation of a thin crystal. The corresonding results can be applied to a restricted set of experimental data related to the cases of no enhancement of the photorefractive response.

Various aspects of the problem of enhancement of the photorefractive response in cubic crystals have been considered in Refs. [4–6,21,22]. The effects of the energy and polarization exchange between the light beams were outside the main line of these studies.

Much effort has been made to describe the additional nonelectro-optic contribution to the photorefractive response caused by the elasto-optic effect [23–29]. The obtained results now allow one to characterize fairly well the photorefractive nonlinearity for various optical configurations and polarizations of the light waves.

There is quite a number of recent publications aimed at the analysis of strong nonlinear effects caused by the enhanced photorefractive response [10,30–33]. Unfortunately, the authors of these papers usually restrict themselves to a formulation of the initial self-consistent equations for wave amplitudes and to particular numerical solutions for these equations. The corresponding numerical results give no general insight into the nonlinear phenomena under study. Moreover, the initial equations often do not include details essential for wave coupling, such as the effect of the polarization switching on the grating amplitude and the elasto-optic effect. A part of the numerical results obtained is outside the field of applicability of the starting equations.

Finally, we mention the papers devoted to the solution of the nonlinear equations for wave coupling in cubic crystals without optical activity as applied to the case of dominating diffusion transport [34,35]. This particular case admits a quite comprehensive analytical treatment, however, it is nowadays mainly of academic interest in view of the weakness of the diffusion mediated photorefractive response.

In this paper we are making an attempt to lay the foundation of an analytical theory of the vectorial wave coupling in cubic photorefractive crystals that are, in general, optically active. The distinctive features of the proposed theory are as follows.

(i) The theory incorporates uniformly all main aspects of 2W coupling: readout, including the effect of optoelasticity; recording, including the enhancement factors; arbitrary orientations of the grating vector and applied field; etc.

(ii) We systematically exploit the properties of spatial symmetry of cubic crystals; this imparts additional generality to the theoretical conclusions and makes them as free as possible from model assumptions.

(iii) We use the apparatus of Pauli matrices to deal with two-dimensional vectors and matrices. The introduction of the Pauli matrices greatly simplifies the structure of the vectorial equations and makes the calculation procedures easy.

(iv) We analyze in detail possible approximations for the nonlinear wave equations, as well as the field of applicability of the obtained results.

(v) The theory is open for further development; deprived of the possibility to exhaust particular results, we often indicate the way to obtain them. As usual, we restrict ourself to the paraxial approximation which is well justified for most experiments.

The structure of the paper is the following. In Sec. II we provide the reader with background information on the optical permittivity of cubic crystals, including optical activity, light absorption, and the linear electro-optic and elasto-optic effects. Then we derive a system of coupled vectorial equations for the wave amplitudes that describes the linear propagation and the mutual Bragg diffraction from a light-induced space-charge grating. The coupled wave equations include the minimum number of phenomenological parameters consistent with the spatial symmetry. In Sec. III we specify the above phenomenological parameters for two general optical configurations and consider the equivalent geometries and a number of important particular cases. The information presented here is sufficient for the description of most configurations relevant to experiment. Section IV is devoted to a summary of the linear properties of light waves in cubic crystals that are necessary for the subsequent theoretical considerations. These properties include the effect of an applied field on the polarization properties of the eigenmodes and on the structure of the corresponding wave surfaces. In Sec. V we give an exact solution of the Bragg-diffraction problem, considering the amplitude of the space-charge grating as a constant. We then apply our results to describe the giant readout pulses during the switching of an applied field; these pulses have been detected recently in ac experiments with BTO crystals [12]. In Sec. VI we describe the photorefractive response of a crystal as applied to two main limiting cases: to the case of diffusion charge transfer and to the case of an applied square-wave field. The obtained explicit relations for the grating amplitude enable us to formulate a closed set of vectorial nonlinear equations for each of the above types of the photorefractive two-wave coupling. In Sec. VII we discuss the approximations appropriate for the diffusion and ac cases, obtain the corresponding simplified equations and solutions for the wave amplitudes, and analyze the polarization properties of the energy exchange. Sec. VIII is devoted to applications of the obtained general results to a description of the angular and polarization dependences of the rate of spatial amplification in BTO crystals, and to a comparison between theory and experiment. A comparison of the main theoretical predictions for BTO crystals with experiment is made in Sec. IX. In Sec. X we discuss the merits of the developed theory and the prospects for its further development and application. The conclusions are drawn in Sec. XI.

II. BASIC RELATIONS

A. Optical permittivity

The known cubic photorefractive crystals belong to point symmetry group 23 (BSO,BTO,BGO, . . .) and $\overline{4}3m$ (GaAs, CdTe,InP, . . .). In the absence of an electric field these crystals are optically isotropic. This isotropy may, however, coexist with optical activity; this is the case for group 23. The electro-optic properties of the above cubic crystals are uniform in symmetry.

For a light wave with wave vector $\vec{k}$ the optical permittivity tensor (ϵ_{ij}) of a cubic crystal, subject to an electric field $\vec{E}$, can be presented in the form

$$\epsilon_{ij}=n_0^2(1+i\,\alpha\,k^{-1})\,\delta_{ij}+2i\,\rho\,n_0^2\,k^{-2}\,\delta_{ijl}k_l+\delta\epsilon_{ij}(\vec{E}), \tag{1}$$

where n_0 is the refractive index, α is the light absorption coefficient, ρ is the rotatory power, δ_{ij} is the unit second rank tensor, and δ_{ijl} is the unit antisymmetric third rank tensor. The Latin subscripts hereafter denote Cartesian components and repeated components in the products' mean summation over *x*, *y*, and *z*. The first two terms in Eq. (1) describe the optical permittivity in the absence of any electric field. The components of the isotropic tensors δ_{ij} and δ_{ijl} are the same in each Cartesian coordinate system. The positive sign of ρ corresponds to the corkscrew rule for the rotation of the polarization plane. In crystals of point group $\overline{4}3m$ the optical activity is absent, $\rho=0$.

The last term in Eq. (1) describes the linear effect of the electric field $\vec{E}$ on the optical permittivity. This term is worthy of special attention. It has been supposed initially that the effect of the electric field is reduced to the so-called linear electro-optic effect, i.e.,

$$\delta\epsilon_{ij}(\vec{E})=-n_0^4\,r_{ijl}\,E_l, \tag{2}$$

where r_{ijl} is the electro-optic third rank tensor. This tensor is real and symmetric in the first two indices; in crystals of point group $\overline{4}3m$ and 23, it is characterized by only one independent component, r_{41}, and may be presented as

$$r_{ijl}=r_{41}\,p_{ijl}^{(0)}, \tag{3}$$

where $p_{ijl}^{(0)}$ is the normalized electro-optic tensor. This tensor is not isotropic; its components look especially simple in the crystallographic coordinate system,

$$p_{ijl}^{(0)}=|\,\delta_{ijl}|. \tag{4}$$

However, it has become clear about ten years ago [23–25] that the dependence $\delta\hat{\epsilon}\,(\vec{E})$ (we use hereafter the sign ''hat'' to mark tensors and matrices) is not described fully by Eq. (2). The point is that the so-called elasto-optic effect can also contribute. The scheme of this additional influence is as follows. The electric field produces a stress inside the crystal owing to the piezoelectric effect and this stress results, in turn, in an independent contribution to $\delta\hat{\epsilon}$. This contribution includes the elasto-optic and piezoelectric coefficients, as well as the elasticity moduli.

The procedure of how to calculate the elasto-optic contribution is described in detail in Refs. [23–28]. In this paper we are merely interested in a simple and effective use of the accumulated results for the description of photorefractive wave mixing. To perform this program we assume that the electric field $\vec{E}$ consists of a uniform part, $\vec{E}_0$, and a spatially oscillating part,

$$\vec{E}=\vec{E}_0+\vec{E}_{\vec{K}}\,e^{i\vec{K}\cdot\vec{r}}+\vec{E}_{\vec{K}}^{\,*}\,e^{-i\vec{K}\cdot\vec{r}}, \tag{5}$$

where $\vec{K}$ is the grating vector, $\vec{E}_{\vec{K}}$ is the complex vectorial grating amplitude, and the asterisk stands for the complex conjugate. Using the linearity of the effect of the electric field on $\delta\hat{\epsilon}$, we have

$$\delta\hat{\epsilon}\,(\vec{E})=\delta\hat{\epsilon}\,(\vec{E}_0)+[\,\delta\hat{\epsilon}\,(\vec{E}_{\vec{K}})\;e^{i\vec{K}\cdot\vec{r}}+\text{c.c.}]. \tag{6}$$

It is essential that the dependences $\delta\hat{\epsilon}\,(\vec{E}_0)$ and $\delta\hat{\epsilon}\,(\vec{E}_{\vec{K}})$ are generally different. Since the uniform field $\vec{E}_0$ does not produce any stress in an unclamped crystal, we can write for this most actual case,

$$\delta\epsilon_{ij}\,(\vec{E}_0)=-n_0^4\,r_{41}\,E_0H_{ij}^{(0)}, \tag{7}$$

where $H_{ij}^{(0)}=H_{ji}^{(0)}=p_{ijl}^{(0)}n_l^0$, E_0 is the amplitude of the applied field, and $\vec{n}^0$ is the unit vector indicating the orientation of $\vec{E}_0$. In the case when $\vec{E}_0$ does not depend on *t*, the vector $\vec{n}^0$ is defined uniquely, $\vec{n}^0=\vec{E}_0/E_0$. In the ac case, when $\vec{E}_0(t)$ changes its sign periodically, the vector $\vec{n}^0$ is defined except for the sign; any choice for $\vec{n}^0$ leads to the same physical results.

The spatially oscillating field indeed produces a stress inside the crystal and this stress depends on the orientation of the vector $\vec{E}_{\vec{K}}$. This vector can, in turn, be written as $\vec{E}_{\vec{K}}=\vec{n}E_{\vec{K}}$, where $E_{\vec{K}}$ is the scalar grating amplitude and $\vec{n}=\vec{K}/K$ is the unit grating vector. Then, for the tensorial amplitude $\delta\hat{\epsilon}\,(\vec{E}_{\vec{K}})$, we can write

$$\delta\epsilon_{ij}(\vec{E}_{\vec{K}})=-n_0^4\,r_{41}\,E_{\vec{K}}H_{ij}, \tag{8}$$

where H_{ij} is a tensor including the electro-optic and elasto-optic contributions. This tensor is also real and symmetric in the indices *i* and *j*. As a rule, the elasto-optic contribution to $\hat{H}$ does not exceed the electro-optic one; hence the elements of the tensor $\hat{H}$ are quantities comparable with or less than one. These quantities are functions of $\vec{n}$ and are known for the main optical configurations relevant to experiment; see also Sec. III. With the elasto-optic contribution neglected we obviously have $H_{ij}=p_{ijl}^{(0)}n_l$. Note that the vector $\vec{n}$ is not generally parallel to $\vec{n}^0$ although, for experiments with external light beams, usually $\vec{n}\|\vec{n}^0$.

Thus the elasto-optic effect renormalizes the electro-optic tensor and this renormalization depends in a known way on the orientation of the grating vector. The field-induced change of the optical permittivity is always anisotropic.

Table I gives representative optical constants for BTO and BSO crystals. These parameters will be used in the following numerical estimates.

B. Two-wave coupling via a space-charge grating

1. Usual representation

Let two light waves, 1 and 2, of the same frequency ω be incident onto the *XY* plane of a crystal. The corresponding electric light field, $\vec{\mathcal{E}}$, inside the crystal may be presented as

$$\vec{\mathcal{E}}=(\vec{A}_1\,e^{i\vec{k}_1\cdot\vec{r}}+\vec{A}_2\,e^{i\vec{k}_2\cdot\vec{r}})\,e^{-i\omega t}+\text{c.c.}, \tag{9}$$

TABLE I. Triplets of basis vectors x,y,z equivalent to $[001],[\bar{1}10],[1\bar{1}0]$ (left column) and $[001],[1\bar{1}0],[110]$ (right column).

x,	y,	z	x,	y,	z
$[001]$,	$[\bar{1}\bar{1}0]$,	$[1\bar{1}0]$	$[001]$,	$[1\bar{1}0]$,	$[110]$
$[001]$,	$[110]$,	$[\bar{1}10]$	$[001]$,	$[\bar{1}10]$,	$[\bar{1}\bar{1}0]$
$[00\bar{1}]$,	$[\bar{1}10]$,	$[110]$	$[00\bar{1}]$,	$[110]$,	$[1\bar{1}0]$
$[00\bar{1}]$,	$[1\bar{1}0]$,	$[\bar{1}\bar{1}0]$	$[00\bar{1}]$,	$[\bar{1}\bar{1}0]$,	$[\bar{1}10]$
$[100]$,	$[0\bar{1}\bar{1}]$,	$[01\bar{1}]$	$[100]$,	$[01\bar{1}]$,	$[011]$
$[100]$,	$[011]$,	$[0\bar{1}1]$	$[100]$,	$[0\bar{1}1]$,	$[0\bar{1}\bar{1}]$
$[\bar{1}00]$,	$[0\bar{1}1]$,	$[011]$	$[\bar{1}00]$,	$[011]$,	$[01\bar{1}]$
$[\bar{1}00]$,	$[01\bar{1}]$,	$[0\bar{1}\bar{1}]$	$[\bar{1}00]$,	$[0\bar{1}\bar{1}]$,	$[0\bar{1}1]$
$[010]$,	$[\bar{1}0\bar{1}]$,	$[\bar{1}01]$	$[010]$,	$[\bar{1}01]$,	$[101]$
$[010]$,	$[101]$,	$[10\bar{1}]$	$[010]$,	$[10\bar{1}]$,	$[\bar{1}0\bar{1}]$
$[0\bar{1}0]$,	$[10\bar{1}]$,	$[101]$	$[0\bar{1}0]$,	$[101]$,	$[\bar{1}01]$
$[0\bar{1}0]$,	$[\bar{1}01]$,	$[\bar{1}0\bar{1}]$	$[0\bar{1}0]$,	$[\bar{1}0\bar{1}]$,	$[101]$
	(a)			(b)	

where the wave amplitudes $\vec{A}_{1,2}$ are slowly varying functions of the propagation coordinate z and the time t; the lengths of the wave vectors, $k_{1,2}$, are equal to $k=\omega n_0/c$ (c is the light velocity). The angles between the wave vectors $\vec{k}_{1,2}$ and the z axis are supposed to be small, which holds true for most photorefractive experiments. Within such a paraxial approximation the amplitudes $\vec{A}_{1,2}$ may be treated as two-dimensional (2D) vectors with x,y components.

The wave vectors' difference $\vec{K}=\vec{k}_1-\vec{k}_2$ is nothing else than the grating vector of the light-induced spatial grating. This vector and the vector $\vec{E}_0$ are supposed to have arbitrary orientations in the XY plane.

Using Eqs. (1), (6), and (8), and the notation introduced in the paraxial approximation, one can obtain from Maxwell equations the following coupled system for the vectorial wave amplitudes $\vec{A}_{1,2}$,

$$\left(\frac{\partial}{\partial z}+\frac{\alpha}{2}\right)\vec{A}_1-i\,\hat{G}\,\vec{A}_1=iE_{\vec{K}}\,\hat{V}\,\vec{A}_2,$$
$$\left(\frac{\partial}{\partial z}+\frac{\alpha}{2}\right)\vec{A}_2-i\,\hat{G}\,\vec{A}_2=iE^*_{\vec{K}}\,\hat{V}\,\vec{A}_1. \tag{10}$$

The matrices $\hat{G}$ and $\hat{V}$ are given by

$$G_{ij}=sE_0\,H^{(0)}_{ij}+i\rho\,\delta_{ijz},$$
$$V_{ij}=s\,H_{ij}, \tag{11}$$

here $s=-\pi n_0^3 r_{41}/\lambda$ is a material parameter and the Latin indices i and j assume independently the values x and y. As is clear from Eqs. (11) and the symmetry properties of the tensors $\hat{H}$ and $\hat{H}^{(0)}$, see the previous subsection, the matrix $\hat{V}$ is real and symmetric, $V_{ij}=V^*_{ij}=V_{ji}$, and the matrix $\hat{G}$ is complex and Hermittian, $G_{ij}=G^*_{ji}$. The sign of the introduced parameter s is opposite to the sign of r_{41} and may be both positive and negative; this sign is often unknown in experiment.

The left-hand sides of Eqs. (10), which are the same for waves 1 and 2, describe linear propagation in the presence of optical activity and field-induced birefringence, whereas the right-hand sides are responsible for the nonlinear coupling. The presence of light absorption yields a common exponential factor $\exp(-\alpha z/2)$ in the expressions for the amplitudes $\vec{A}_{1,2}$. It does not affect the polarization properties and, if required, may be taken into account in the final expressions for $\vec{A}_{1,2}$. For simplicity, from now on we omit the terms $\alpha\vec{A}_{1,2}/2$ in Eqs. (10). One can check thereafter that the total intensity $I_0=|\vec{A}_1|^2+|\vec{A}_2|^2$ remains constant across the crystal. This is an obvious generalization of the known conservation law for the scalar two-wave coupling.

Up to this point our treatment of the vectorial two-wave coupling was not much different from the treatment by other authors. Below we are creating a step to unify and simplify the set (10) using the technique of Pauli σ matrices [35,36].

2. σ representation

The apparatus of σ matrices is an ideal tool to deal with 2D vectors and matrices. Three σ matrices (operators), $\hat{\sigma}_1,\hat{\sigma}_2,\hat{\sigma}_3$, which may formally be considered components of the vectorial operator $\hat{\vec{\sigma}}$, are defined by the expressions

$$\hat{\sigma}_1=\begin{pmatrix}0&1\\1&0\end{pmatrix},\qquad \hat{\sigma}_2=\begin{pmatrix}0&-i\\i&0\end{pmatrix},\qquad \hat{\sigma}_3=\begin{pmatrix}1&0\\0&-1\end{pmatrix}. \tag{12}$$

These Hermitian matrices possess a number of remarkable mathematical properties. The most fundamental of them is the relation

$$\hat{\sigma}_\alpha\hat{\sigma}_\beta=\delta_{\alpha\beta}\hat{1}+i\,\delta_{\alpha\beta\gamma}\hat{\sigma}_\gamma, \tag{13}$$

where $\hat{1}$ is the unit 2×2 matrix and each of the Greek indices α, β, and γ takes the values 1, 2, and 3 (do not mix these up with the Latin indices i and j taking the values x, y , z). As follows from Eq. (13), any combination (function) of the σ matrices is reduced to a linear combination of them. In particular, the following equivalent of the known Euler formula is valid for the σ matrices [35,36],

$$e^{i\vec{\varphi}\cdot\hat{\vec{\sigma}}}=\hat{1}\cos\varphi+i\,\frac{\vec{\varphi}\cdot\hat{\vec{\sigma}}}{\varphi}\sin\varphi, \tag{14}$$

where $\vec{\varphi}=(\varphi_1,\varphi_2,\varphi_3)$ is a real 3D vector (not to be mixed up hereafter with vectors in the coordinate x, y, z space) and φ is its length. The definition of the matrix exponent,

$$\exp(\hat{U})=\hat{1}+\frac{1}{1!}\hat{U}+\frac{1}{2!}\hat{U}^2+\cdots, \tag{15}$$

is similar to the definition of the scalar exponent $\exp(U)$ with help from the Taylor series.

An arbitrary 2×2 complex matrix $\hat{U}$ may be expressed by $\hat{1}$ and $\hat{\vec{\sigma}}$,

$$\hat{U}=c_0\,\hat{1}+\vec{c}\cdot\hat{\vec{\sigma}}, \tag{16}$$

where $c_0=\frac{1}{2}\,\mathrm{Tr}\,(\hat{U})$, $\vec{c}=\frac{1}{2}\,\mathrm{Tr}\,(\hat{\vec{\sigma}}\,\hat{U})$, and Tr means the taking of the matrix trace. The derivation of this relation exploits Eq. (13) and the fact that $\mathrm{Tr}\,(\hat{\vec{\sigma}})=0$. Actually, Eq. (16) represents the decomposition of the matrix $\hat{U}$ into the isotropic and the anisotropic parts. In the case when $\hat{U}$ is a Hermitian matrix, the constant c_0 and the vector $\vec{c}=(c_1,c_2,c_3)$ are real quantities.

Using the above mathematical properties, we present the matrices $\hat{G}$ and $\hat{V}$, given by Eqs. (11), in the canonical form,

$$\hat{G}=\vec{\kappa}\cdot\hat{\vec{\sigma}},\quad \hat{V}=\nu_0\hat{1}+\vec{\nu}\cdot\hat{\vec{\sigma}}, \tag{17}$$

where the real scalar parameter ν_0 and the real vectors $\vec{\nu}=(\nu_1,\nu_2,\nu_3)$ and $\vec{\kappa}=(\kappa_1,\kappa_2,\kappa_3)$ are given by

$$\nu_0=s(H_{xx}+H_{yy})/2,$$

$$\nu_1=sH_{xy},\quad \nu_2=0,\quad \nu_3=s(H_{xx}-H_{yy})/2, \tag{18}$$

$$\kappa_1=sE_0H_{xy}^{(0)},\quad \kappa_2=-\rho,\quad \kappa_3=sE_0(H_{xx}^{(0)}-H_{yy}^{(0)})/2.$$

As was stated earlier, the parameter s is given by $s=-\pi n_0^3 r_{41}/\lambda$.

Correspondingly, Eqs. (10), with light absorption neglected, attain the final form,

$$\left(\frac{\partial}{\partial z}-i\vec{\kappa}\cdot\hat{\vec{\sigma}}\right)\vec{A}_1=iE_K(\nu_0+\vec{\nu}\cdot\hat{\vec{\sigma}})\vec{A}_2,$$

$$\left(\frac{\partial}{\partial z}-i\vec{\kappa}\cdot\hat{\vec{\sigma}}\right)\vec{A}_2=iE_K^{*}(\nu_0+\vec{\nu}\cdot\hat{\vec{\sigma}})\vec{A}_1. \tag{19}$$

The information about the linear properties of the light waves is now included in the vector $\vec{\kappa}$, whereas the parameters $\vec{\nu}$ and ν_0 characterize the wave coupling. Generally speaking, the matrix $\hat{G}$ also has an isotropic contribution $sE_0(H_{xx}^{(0)}+H_{yy}^{(0)})\,\hat{1}/2$. This contribution gives, however, only a small renormalization of the refractive index n_0, which usually leads to no significant effects. The presence of the parameter ν_0 on the right-hand side of Eq. (19) has an important meaning, namely, that the wave interaction has an isotropic part.

The matrix elements H_{ij} and $H_{ij}^{(0)}$ entering Eqs. (18) are some dimensionless parameters of the order of one, depending on the orientation of the vectors $\vec{n}$ and $\vec{n}^{\,0}$ in the XY plane. For the cases relevant to experiment we calculate these parameters below in Sec. III. It is remarkable that the ratios ν_1/ν_3 and κ_1/κ_3 may be different owing only to the elasto-optic contribution to $\delta\hat{\epsilon}(\vec{E})$ and a nonzero angle between $\vec{n}$ and $\vec{n}^{\,0}$. Otherwise, we find from Eqs. (18) that $(\vec{\nu}\times\vec{\kappa})=0$.

The strengths of the effects of optical activity and field-induced birefringence are determined by the parameters $|\rho|$ and $|sE_0|$, respectively. The value zero of ν_2 in Eqs. (18) means that the space-charge field does not affect the optical activity.

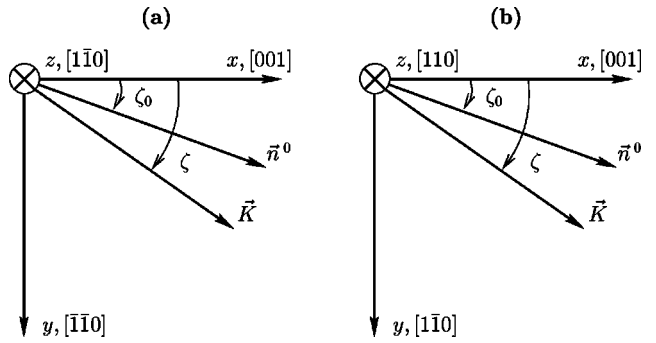

FIG. 1. Two basic nonequivalent configurations for 2W coupling in cubic crystals.

III. MAIN OPTICAL CONFIGURATIONS

A. Two basic configurations

Most optical configurations relevant to experiment may be described uniformly with the help of the geometrical scheme shown in Fig. 1(a). The propagation axis z coincides with the crystal axis $[1\bar{1}0]$, the x and y axes are directed along $[001]$ and $[\bar{1}10]$, respectively, and the azimuth angles in the XY plane are measured from the principal axis $[001]$ in the direction that is standard for a polar coordinate system. In the general case, the angles ζ_0 and ζ that define the orientations of the vectors $\vec{E}_0$ and $\vec{K}$ are different.

Figure 1(b) shows another optical configuration that is not equivalent to the previous one because its basis vectors cannot be made coincident with the basis vectors of Fig. 1(a) by the symmetry transformations of the point group 23 and $\bar{4}3m$ (see also below in this section). The photorefractive manifestations are generally different for these nonequivalent configurations analogously to the difference in photorefractive phenomena in ferroelectrics for opposite directions of the polar axis. Mathematically, the transition from one configuration to the other is expressed by the multiplication of the matrices $\hat{H}$ and $\hat{H}^{(0)}$ by a factor of -1. It is therefore sufficient to describe the dependences $H_{ij}(\zeta)$ and $H_{ij}^{(0)}(\zeta_0)$ for the basic configuration shown in Fig. 1(a).

For the optical configuration depicted in Fig. 1(a) the matrix $\hat{H}^{(0)}(\zeta_0)$, characterizing the change of the optical permittivity owing to the applied uniform field, has a simple form,

$$H_{ij}^{(0)}=\begin{pmatrix}0 & \sin\zeta_0\\ \sin\zeta_0 & \cos\zeta_0\end{pmatrix}. \tag{20}$$

Using Eqs. (18), we easily calculate the parameters $\kappa_{1,3}$ as functions of ζ_0,

$$\kappa_1=sE_0\sin\zeta_0,\quad \kappa_3=-\frac{sE_0}{2}\cos\zeta_0. \tag{21}$$

The elasto-optic contributions make the angular dependences $H_{ij}(\zeta)$ more complicated in comparison with $H_{ij}^{(0)}(\zeta_0)$. Figure 2 shows these dependences for BTO and BSO crystals obtained on the basis of the literature data [24,28]. The nonperturbed dependences $H_{ij}^{(0)}(\zeta)$ are also shown for comparison.

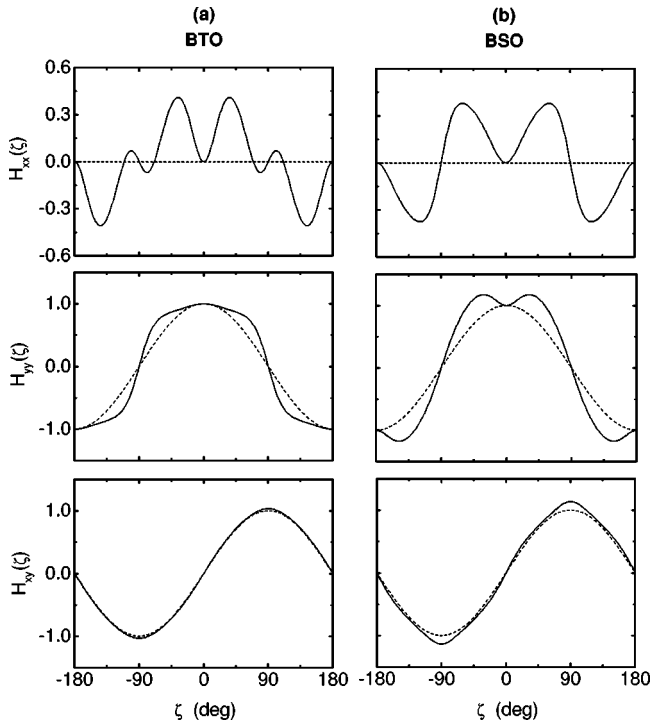

FIG. 2. Dependences of the matrix elements $H_{ij}(\zeta)$ for BTO (a) and BSO (b) crystals; the dashed lines correspond to the nonperturbed functions.

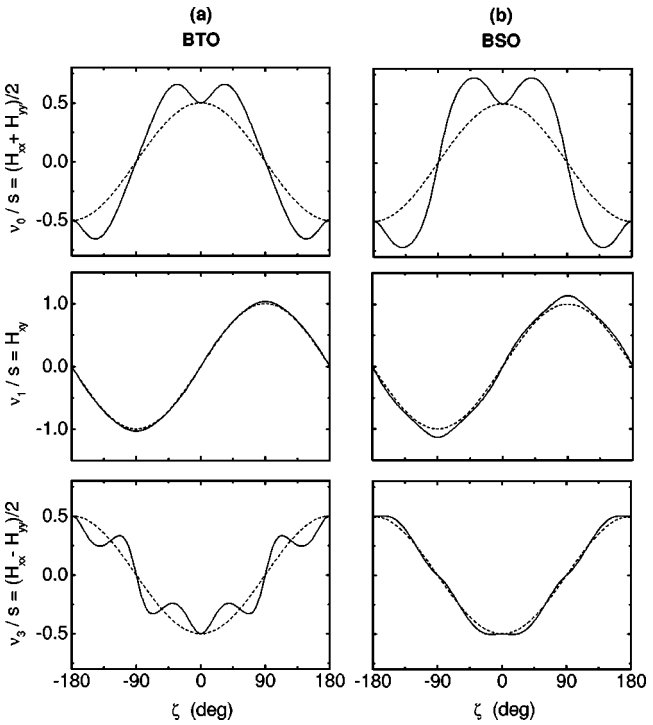

FIG. 3. Dependences $\nu_{0,1,3}(\zeta)$ for BTO (a) and BSO (b) crystals.

It is important that the following symmetry properties hold true for the elements of the $\hat{H}$ matrix,

$$H_{xx}(\zeta)=H_{xx}(-\zeta), \quad H_{yy}(\zeta)=H_{yy}(-\zeta),$$
$$H_{xy}(\zeta)=-H_{xy}(-\zeta), \tag{22}$$
$$H_{ij}(\zeta)=-H_{ij}(\zeta\pm\pi).$$

These properties are clearly seen in Fig. 2. They follow, as it may be proven, from the properties of spatial symmetry of the crystals of the point group 23 and $\bar{4}3m$. As seen from Eqs. (18) and Eq. (22), the function $\nu_1(\zeta)$ is odd, whereas the functions $\nu_0(\zeta)$ and $\nu_3(\zeta)$ are even (see also Fig. 3).

To gain a preliminary impression of the role of the elasto-optic contributions, we look again at Fig. 2. One sees that these contributions cannot be neglected in the general case. On the other hand, they dominate only in rare cases. We can expect that the elasto-optic contributions are most important in the cases when the conventional electro-optic effect fails occasionally to provide the wave coupling. Otherwise, the optoelasticity should give only moderate corrections to the coupling characteristics. Note that for some special orientations of the grating vector the elasto-optic contributions turn to zero (see Figs. 2 and 3, and also below in this section).

With neglected elasto-optic contributions we have $\hat{H}(\zeta)=\hat{H}^{(0)}(\zeta)$ and, correspondingly,

$$\nu_0=\frac{s}{2}\cos\zeta, \quad \nu_1=s\sin\zeta, \quad \nu_3=-\frac{s}{2}\cos\zeta. \tag{23}$$

These expressions are useful for rough calculations.

B. Particular optical configurations and cases

For experiments with applied electric fields, optical configurations are defined by the orientation of the field vector $\vec{E}_0$ with respect to the crystal axes. Four particular configurations, which correspond to different values of the angle ζ_0 in Fig. 1(a), are of particular interest [2,13,24]: (i) the longitudinal configuration $\vec{E}_0\|[001]$, i.e., $\sin\zeta_0=0$; (ii) the transversal configuration $\vec{E}_0\perp[001]$, i.e., $\cos\zeta_0=0$; (iii) the diagonal configuration $\vec{E}_0\|[\bar{1}\bar{1}1]$; here $\zeta_0=\arctan(\sqrt{2})$, i.e., $\zeta_0\simeq 54.7°$ or $-125.3°$; and (iv) the diagonal configuration $\vec{E}_0\|[111]$; here $\zeta_0=-\arctan(\sqrt{2})$, i.e., $\zeta_0\simeq -54.7°$ or $125.3°$. The above diagonal configurations are similar but not equivalent (see this in more detail in Sec. VIII).

As we have mentioned, the grating vector $\vec{K}$ is not parallel to $\vec{E}_0$ in the general case. This is relevant to the studies of wide-angular light-induced scattering (fanning), which is due to the recording of a variety of noise gratings by a pump wave and weak seed waves. For experiments with external light beams, as a rule, $\vec{K}$ is parallel to $\vec{E}_0$. Keeping in mind this actual situation we consider four particular cases [see also Fig. 1(a)].

(i) *The fully longitudinal case,* $\vec{K}\|\vec{E}_0\|[001]$, *i.e.,* $\sin\zeta=\sin\zeta_0=0$. In this geometry the elasto-optic contribution is absent, $\hat{H}=\hat{H}^{(0)}$, and the only nonzero component of $\hat{H}^{(0)}$ is $H^{(0)}_{yy}=\pm 1$. Correspondingly, we have here $\nu_0=\pm s/2$, $\nu_1=0$, and $\nu_3=\mp s/2$.

(ii) *The fully transversal case,* $\vec{K}\|\vec{E}_0\perp[001]$, *i.e.,* $\cos\zeta=\cos\zeta_0=0$. Here the diagonal elements H_{xx} and H_{yy} remain equal to zero ($\nu_0=\nu_3=0$) and the elasto-optic contribution moderately renormalizes the value of the nondiagonal matrix elements $H_{xy}\equiv H_{yx}$ as compared with $H^{(0)}_{xy}\equiv H^{(0)}_{yx}=\pm 1$.

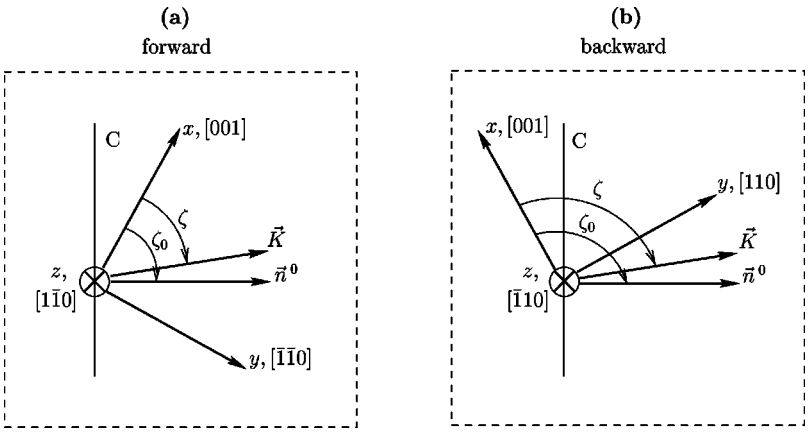

FIG. 4. Geometrical schemes for the forward (a) and the backward (b) optical configurations; the dashed lines depict the crystal faces.

(iii) *The fully diagonal cases,* $\vec{K}\|\vec{E}_0\|[\overline{111}]$ *and* $\vec{K}\|\vec{E}_0\|[111]$. Here $\tan\zeta=\tan\zeta_0=\pm\sqrt{2}$; in the diagonal geometries the elasto-optic contributions are clearly pronounced (see Figs. 2 and 3).

C. Equivalent configurations

For any cubic crystal of the point group 23 or $\bar{4}3m$ there are 12 symmetry transformations that do not affect its macroscopic properties [35,37,38]. In addition to the trivial unit transformation these are 180° rotations around three principal crystal axes, ±120° rotations around four principal diagonals, and combinations of these symmetry tranformations. Therefore, we can immediately indicate eleven optical configurations equivalent to the one shown in Fig. 1(a). Table I(a) gives the corresponding triplets of the basis x,y,z vectors for all equivalent configurations. Any of these triplets may be used as the basis vectors of the Cartesian right-handed coordinate system. The first line of Table I(a) corresponds to the coordinate system shown in Fig. 1(a). Analogously, Table I(b) lists the optical configurations equivalent to the one shown in Fig. 1(b). The sets entering Tables I(a) and I(b) have no overlap. The introduced notion of equivalent and nonequivalent optical configurations and the above formulated method for their description considerably extend the capability of our theory.

Using the properties of spatial symmetry, one can easily prove the identity of the characteristics of the so-called forward and backward 2W coupling. This fact is important for the interpretation of the available data on light-induced scattering and the description of schemes of optical generation based on four-wave mixing. Let us assume, see Fig. 4, that a backward configuration is obtained from an initial foward configuration by means of a 180° rotation of the sample around an arbitrary *C*-axis lying in the *XY*-plane. In experiment this axis is parallel (perpendicular) to certain crystal faces. As seen from Fig. 2 and the first two lines of Table I(a), the backward configuration is equivalent to the forward one. Therefore all the angular characteristics of 2W coupling must be the same for the above configurations. This merely means that the forward and backward directions are physically equivalent in harmony with the reciprocity principle [41]. It is assumed indeed that all of the angles for the forward and backward configurations are measured from the *x* axis directed along the corresponding principal axis of the crystal [see Figs. 4(a) and 4(b)].

In experiment, the *C* axis is usually perpendicular to the applied field. In this case, as one can see from Fig. 4, the angle ζ_0 between the applied field and the *x* axis is different for the forward and backward configurations. Therefore the ζ dependences for 2W mixing should not be the same. This difference has, however, nothing to do with nonequivalence of the forward and backward directions. In Sec. VIII we analyze the orientation characteristics of 2W coupling for forward and backward optical configurations in more detail as applied to experiments with BTO crystals.

IV. LINEAR PROPERTIES OF LIGHT WAVES

Let us first apply Eqs. (19) to describe the light eigenmodes in the absence of wave mixing. Omitting the terms on the right-hand side and putting the wave amplitude $\vec{A}\propto\exp(i\delta k z)$, we come to the following linear algebraic eigenvalue problem for each of two waves,

$$(\vec{\kappa}\cdot\hat{\vec{\sigma}})\vec{A}=\delta k\,\vec{A}. \tag{24}$$

Since the operator $(\vec{\kappa}\cdot\hat{\vec{\sigma}})$ is Hermitian, Eq. (24) admits two real eigenvalues $\delta k_\pm$, which are nothing but corrections to the length of the wave vector *k* for two eigenlightwaves, (+) and (–). One can find directly from Eq. (24) that

$$\delta k_\pm=\pm\kappa; \tag{25}$$

therefore, the distance between the wave surfaces is 2κ within the paraxial approximation.

The eigenvectors $\vec{A}_\pm$, that correspond to the eigenvalues $\delta k_\pm$ and define the polarization states of the $(\pm)$ modes, are given by

$$\vec{A}_\pm=(\hat{1}\pm\vec{o}\cdot\hat{\vec{\sigma}})\vec{A}^0, \tag{26}$$

where $\vec{o}=\vec{\kappa}/\kappa$ is the unit vector along $\vec{\kappa}$, and $\vec{A}^0$ is an arbitrary 2D vector. This relation may be verified algebraically using the identity $(\vec{o}\cdot\hat{\vec{\sigma}})^2\equiv\hat{1}$. The eigenvectors $\vec{A}_\pm$ are, as usual, not defined uniquely which is, however, of no importance for the characterization of the polarization states [39,40]. By choosing $A^0_x=1$, $A^0_y=0$ and introducing the unit polarization vectors $\vec{e}_\pm=\vec{A}_\pm/|\vec{A}_\pm|$, we obtain the following explicit relation:

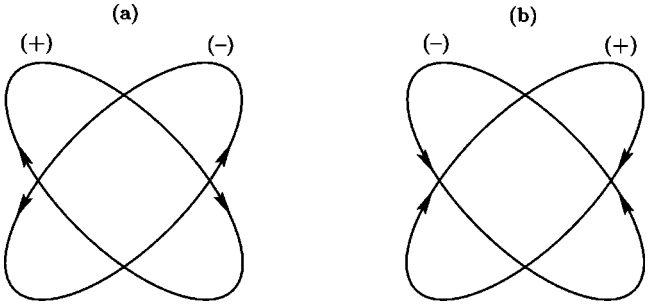

FIG. 5. Polarization ellipses for $(\pm)$ eigenmodes before (a) and after (b) switching of an applied field.

$$\vec{e}_{\pm}=\frac{1}{\sqrt{2\kappa}}\begin{pmatrix}\sqrt{\kappa\pm\kappa_3}\\ \pm\dfrac{\kappa_1+i\kappa_2}{\sqrt{\kappa\pm\kappa_3}}\end{pmatrix}. \tag{27}$$

Obviously the polarization vectors $\vec{e}_{\pm}$ are orthogonal to each other, $\vec{e}_{+}^{\,*}\cdot\vec{e}_{-}=0$.

The eigenvectors $\vec{e}_{\pm}$ fully describe the polarization states of the $(\pm)$ eigenmodes. Generally, these vectors are complex, i.e., the eigenwaves are elliptically polarized; the large axes of the ellipses are mutually orthogonal and the rotation directions are opposite each other (see Fig. 5). In the absence of an applied field we have $\kappa_{1,3}=0$; this corresponds to the left and right circularly polarized eigenwaves. If optical activity is neglected, the eigenvectors $\vec{e}_{\pm}$ become real; that is, the eigenwaves become linearly polarized. For sufficiently large applied fields, $|sE_0|\gg|\rho|$, the degree of the ellipticity becomes as small as $(\rho/sE_0)^2$.

From Eqs. (18) and (27) we obtain the relation

$$\vec{e}_{\pm}(-E_0)=\vec{e}_{\mp}^{\,*}(E_0), \tag{28}$$

which is useful for the analysis of the photorefractive response in the presence of an applied ac field (see Sec. VI). This relation means that switching of the applied field results in switching of the large and small ellipse axes without any change of the rotation directions (see Fig. 5).

The linear differential equation for the wave amplitude $\vec{A}(z)$,

$$\frac{d\vec{A}}{dz}=i(\vec{\kappa}\cdot\hat{\vec{\sigma}})\vec{A}, \tag{29}$$

which follows from Eqs. (19), allows one to describe the linear wave propagation for an arbitrary input amplitude $\vec{A}(0)$. The corresponding solution is

$$\vec{A}(z)=e^{i(\vec{\kappa}\cdot\hat{\vec{\sigma}})z}\vec{A}(0)\equiv[\hat{1}\cos\kappa z+i(\vec{o}\cdot\hat{\vec{\sigma}})\sin\kappa z]\vec{A}(0). \tag{30}$$

One sees that the amplitude $\vec{A}$ is generally a superposition of two eigenmodes. In order to excite only one eigenmode inside the crystal, one should use an elliptically polarized input wave with the amplitude $\vec{A}(0)$ proportional to one of the eigenvectors $\vec{e}_{\pm}(E_0)$. If the input amplitude $\vec{A}(0)$ is real (i.e., the input wave is linearly polarized), we obtain the relation $\vec{A}(-E_0,z)=\vec{A}^{\,*}(E_0,z)$ from Eq. (30). This signals a change of sign of the polarization rotation at each point of the crystal when switching the applied field.

Although Eq. (30) for the complex amplitude $\vec{A}$ fully characterizes the evolution of the polarization state along the crystal, it is useful to represent it in an equivalent form by introducing the so-called Stokes parameters ξ_1,ξ_2,ξ_3 [39,41]. These real parameters, which may be considered as componets of the Stokes vector $\vec{\xi}$, are ideally compatible with the apparatus of σ matrices; they can describe uniformly the polarization properties of totally and partially polarized waves. The Stokes vector $\vec{\xi}$ is defined as $\vec{\xi}=\mathrm{Tr}(\hat{\vec{\sigma}}\hat{\Pi})$, where $\Pi_{\alpha\beta}=A_\alpha A_\beta^*/I_0$ is the polarization matrix. This definition of $\vec{\xi}$ corresponds to the representation of the $\hat{\Pi}$ matrix in the form $\hat{\Pi}=\frac{1}{2}(\hat{1}+\vec{\xi}\cdot\hat{\vec{\sigma}})$. The parameters $\xi_{1,3}$ characterize the degree of linear polarization and the parameter ξ_2 characterizes the degree of ellipticity. For a totally polarized wave (which is our only interest in this paper) the length of the Stokes vector $\xi=|\vec{\xi}|$ equals one. If, in addition, this wave is polarized linearly with an inclination angle φ to the x axis we have $\xi_1=\sin 2\varphi$, $\xi_2=0$, and $\xi_3=\cos 2\varphi$.

Using Eqs. (13) and (30), we can find the dependence of the Stokes vector on the propagation coordinate,

$$\vec{\xi}=\vec{\xi}_0\cos 2\kappa z+(\vec{\xi}_0\times\vec{o})\sin 2\kappa z+2\vec{o}(\vec{o}\cdot\vec{\xi}_0)\sin^2\kappa z, \tag{31}$$

where $\vec{\xi}_0=\vec{\xi}(0)$ is the input Stokes vector. One sees that the z dependence of the polarization state is defined by the mutual orientation of the vectors $\vec{\xi}_0$ and $\vec{o}=\vec{\kappa}/\kappa$. If $\vec{\xi}_0=\pm\vec{o}$, which corresponds to $\vec{A}(0)\propto\vec{e}_{\pm}$, the polarizion state remains unchanged during the linear propagation.

V. EXACT SOLUTION OF THE BRAGG-DIFFRACTION PROBLEM

Equations (19) enable us to easily obtain the exact solution for the wave amplitudes $\vec{A}_{1,2}$ in the case when the grating amplitude $E_{\vec{K}}$ does not depend on the propagation coordinate z. In particular, we can easily describe the diffraction efficiency of a spatially uniform grating, as well as the polarization properties of the diffracted wave without any restrictions on the crystal thickness l, the value of the grating amplitude $|E_{\vec{K}}|$, and the rotatory power ρ [16]. To find the exact solution, we introduce new variables $\vec{B}_{\pm}=\vec{A}_1\exp(-i\phi_0)\pm\vec{A}_2$ instead of $\vec{A}_{1,2}$, where $\phi_0=\arg(E_{\vec{K}})$ is a constant phase. As a result, from Eqs. (19) we arrive at two independent linear equations for $\vec{B}_+$ and $\vec{B}_-$. The explicit solution of these equations is

$$\vec{B}_{\pm}(z)=e^{i\hat{g}_{\pm}z}\vec{B}_{\pm}(0), \tag{32}$$

where $\hat{g}_{\pm}=\vec{\kappa}\cdot\hat{\vec{\sigma}}\pm|E_{\vec{K}}|(\nu_0\hat{1}+\vec{\nu}\cdot\hat{\vec{\sigma}})$. From Eq. (32) and the definition of $\vec{B}_{\pm}$ we obtain the sought solution for $\vec{A}_{1,2}$,

$$A_{1,2}(z)=\hat{T}_{+}(z)\vec{A}_{1,2}(0)+e^{\pm i\phi_0}\hat{T}_{-}(z)\vec{A}_{2,1}(0), \tag{33}$$

where the transformation matrices $\hat{T}_{\pm}(z)$ are given by

$$\hat{T}_{\pm}(z)=\frac{1}{2}(e^{i\hat{g}_{+}z}\pm e^{i\hat{g}_{-}z}). \tag{34}$$

To describe the diffraction of wave 1 from the grating, one should put $\vec{A}_2(0)=0$ and calculate $\vec{A}_2(l)$. From Eq. (33) we get

$$\vec{A}_2(l)=e^{-i\phi_0}\hat{T}_{-}(l)\,\vec{A}_1(0). \tag{35}$$

The phase factor $\exp(i\phi_0)$ entering this expression affects neither the diffraction efficiency, $\eta=|\vec{A}_2(l)|^2/|\vec{A}_1(0)|^2$ nor the polarization state of the diffracted wave 2. Using Eq. (14), the matrix $\hat{T}_{-}$ may be presented as

$$\hat{T}_{-}=a\,\hat{1}+\vec{b}\cdot\hat{\vec{\sigma}}. \tag{36}$$

The scalar a and the 3D vector $\vec{b}=(b_1,b_2,b_3)$ are given by

$$a=\frac{1}{2}(e^{i|E_{\vec{K}}|\nu_0 l}\cos\kappa_{+}l-e^{-i|E_{\vec{K}}|\nu_0 l}\cos\kappa_{-}l),$$
$$\vec{b}=\frac{i}{2}(\vec{o}_{+}e^{i|E_{\vec{K}}|\nu_0 l}\sin\kappa_{+}l-\vec{o}_{-}e^{-i|E_{\vec{K}}|\nu_0 l}\sin\kappa_{-}l), \tag{37}$$

where $\vec{\kappa}_{\pm}=\vec{\kappa}\pm|E_{\vec{K}}|\vec{\nu}$ and $\vec{o}_{\pm}=\vec{\kappa}_{\pm}/\kappa_{\pm}$.

Let $\vec{\xi}_1(0)$ be the Stokes vector for input wave 1. Then, using Eq. (13) and the definition of the Stokes vector given in the previous section, the diffraction efficiency η and the Stokes vector $\vec{\xi}_2(l)$ for the diffracted wave 2 may be expressed through the known parameters a and $\vec{b}$ as follows:

$$\eta=|a|^2+|\vec{b}|^2+\vec{\xi}_1(0)\cdot(a\,\vec{b}^{\,*}+a^*\,\vec{b}+i\,\vec{b}^{\,*}\cdot\vec{b}),$$
$$\eta\vec{\xi}_2(l)=i\,\vec{b}\cdot\vec{b}^{\,*}+(|a|^2-|\vec{b}|^2)\,\vec{\xi}_1(0)+[a^*\vec{b}+ia^*\vec{b}\cdot\vec{\xi}_1(0)$$
$$+\vec{b}(\vec{b}^{\,*}\cdot\vec{\xi}_1(0))+\text{c.c.}]. \tag{38}$$

These equalities give the general solution to the Bragg-diffraction problem. This solution incorporates, in particular, the influence of the elasto-optic effect. It includes, actually, a great deal of information on the polarization, orientation and field dependence of η and $\vec{\xi}$.

As an application of Eqs. (38) we consider a simple example relevant to recent ac-experiments with fiberlike BTO crystals [12]. Figure 6 shows the normalized dependences $\eta(E_0;l)$ for the longitudinal optical configuration $(\vec{K}\|\vec{E}_0)$ and the input linear polarization parallel to the x axis. These dependences correspond to Eqs. (37) and (38), and the BTO parameters given in Table II. One sees that increasing $|E_0|$ leads to a remarkable decrease in the diffraction efficiency. The larger the thickness l, the sharper the peak of $\eta(E_0)$. For $l=15$ mm and $|E_0|=30$ kV/cm, which is typical of the above experiments, the ratio $\eta(0)/\eta(|E_0|)$ is as high as 30.

The described feature has a clear physical meaning and important implications. Since in the longitudinal geometry only the yy-component of the interaction matrix $\hat{V}$ is nonzero [see Eqs. (11) and (20)], diffraction of an initially x-polarized wave is possible only after a rotation of the polarization plane owing to optical activity. However, a sufficiently large applied field, $|sE_0|\gg|\rho|$, strongly suppresses this rotation because it makes the eigenwaves nearly linearly polarized in the x and the y directions [see Eq. (27)]. For this reason (i) the diffraction efficiency η remains very low and (ii) the wave coupling cannot significantly affect the buildup of the spatial grating. During switching of a square-wave field (when $|sE_0|\lesssim|\rho|$) the recorded grating becomes instantly highly diffractive. In other words, the processes of nonperturbing recording and efficient readout become separated in time. The most obvious manifestations of this effect are giant readout pulses during switching of a square-wave ac-field in 2W-mixing experiments with fiberlike BTO crystals [12].

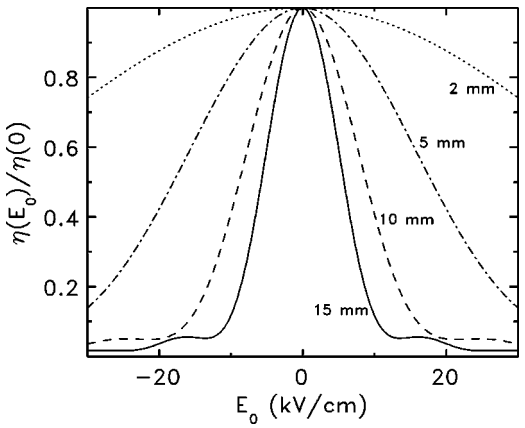

FIG. 6. Normalized diffraction efficiency η versus E_0 for different crystal thickness l.

VI. PHOTOREFRACTIVE RESPONSE

To be able to fully describe the photorefractive 2W coupling, we should supplement Eqs. (19) for the wave amplitudes by relations for the photorefractive response expressing the grating amplitude $E_{\vec{K}}$ through $\vec{A}_{1,2}$. Using the conventional one-trap–one-band model for the charge transfer [1–3] and assuming provisionally that the applied field is parallel to the grating vector (i.e., $\zeta=\zeta_0$ in Fig. 1) we have, within the linear approximation in the contrast of the light pattern,

$$\frac{\partial E_K}{\partial t}+\frac{1}{\tau_d}\frac{E_M}{E_q}\frac{E_q+E_D-iE_0}{E_M+E_D-iE_0}E_K$$
$$=-\frac{\vec{A}_1\cdot\vec{A}_2^{*}}{I_0}\frac{1}{\tau_d}\frac{E_M(E_0+iE_D)}{E_M+E_D-iE_0}. \tag{39}$$

TABLE II. Optical parameters of BTO and BSO crystals.

Parameters	BTO ($\lambda=633$ nm)	BSO ($\lambda=514$ nm)	BSO ($\lambda=633$ nm)
Refractive index, n_0	2.58	2.6	2.54
Rotatory power, ρ	6.5 deg/mm $\simeq 1.13$ cm^{-1}	38.6 deg/mm $\simeq 6.74$ cm^{-1}	21.4 deg/mm $\simeq 3.73$ cm^{-1}
Electro-optic coefficient, r_{41}	4.74 pm/V	4.51 pm/V	4.41 pm/V

TABLE III. Material parameters for BTO and BSO crystals.

Parameters	BTO	BSO
Effective trap density, N_t	2×10^{16} cm^{-3}	10^{16} cm^{-3}
Mobility-lifetime product, $\mu\tau$	2×10^{-7} cm^2/V	5×10^{-7} cm^2/V
Dielectric constant, ε	47	56

Here τ_d is the dielectric relaxation time, $I_0=|\vec{A}_1|^2+|\vec{A}_2|^2$ is the total intensity, and E_D, E_q, and E_M are the characteristic fields,

$$E_D=\frac{Kk_BT}{e}, \qquad E_q=\frac{eN_t}{\epsilon\epsilon_0K}, \qquad E_M=\frac{1}{K\mu\tau}, \quad (40)$$

where e is the elementary charge, k_B is the Boltzmann constant, T is the absolute temperature, N_t is the effective trap concentration, $\epsilon\epsilon_0$ is the dielectric constant, and $\mu\tau$ is the mobility-lifetime product for photoelectrons. The dielectric relaxation is usually due to the photoconductivity caused by photoexcited electrons. In this case

$$\frac{1}{\tau_d}=\frac{e}{\epsilon\epsilon_0}\frac{\alpha I_0}{\hbar\omega}\mu\tau, \quad (41)$$

where $\hbar\omega$ is the energy of a light quantum and α is the light absorption coefficient.

Now we want to generalize Eq. (39) to the case when $\vec{K}$ is not parallel to $\vec{E}_0$; this is important for the description of light-induced scattering. To obtain the desired result it is sufficient to replace in Eq. (39) the amplitude E_0 by the longitudinal (with respect to $\vec{K}$) field component, $E_0 \rightarrow E_0\cos\psi$, where $\cos\psi=\vec{n}\cdot\vec{n}^0$ and $\vec{n}$ and $\vec{n}^0$ are again the unit grating and field vectors. Actually, $E_0\cos\psi$ is the driving field for the grating formation.

Table III gives a representative set of material parameters for BTO and BSO crystals and Table IV lists the corresponding numerical estimates for the characteristic fields. It is seen that the following inequalities are fulfilled with a large safety margin:

$$E_q \gg E_D, E_M, \qquad E_q \gtrsim |E_0|. \quad (42)$$

These inequalities define most of the characteristic features of the sillenites.

We consider below two important limiting cases for the photorefractive response: the case of zero applied field and the case of a strong square-wave ac field. If $E_0=0$, Eq. (39) gives the simplest expression for the steady-state photorefractive response

$$E_K=-i\tilde{E}_D(\vec{A}_1\cdot\vec{A}_2^*)/I_0, \quad (43)$$

where $\tilde{E}_D=E_D(1+E_D/E_q)^{-1}$. This formula shows that the spatial grating is $\pi/2$ shifted with respect to the light fringes. The maximum value of $\tilde{E}_D$ as a function of K occurs at $KR_d=1$, where $R_d=(\epsilon\epsilon_0k_BT/N_te^2)^{1/2}$ is the Debye screening length. For the BSO parameters given in Table III we obtain $K_{max}\simeq1.3\times10^5$ cm^{-1} and $\tilde{E}_D^{max}\simeq3$ kV/cm. A similar estimate is valid for BTO crystals. The photorefractive response in the diffusion case is fairly weak.

The case of a square-wave ac field is worth a more detailed consideration. It is supposed that the oscillation period of $E_0(t)$ is much shorter than the characteristic buildup time of the space-charge field which is, in turn, comparable with τ_d. Therefore, we can perform an averaging of Eq. (39) over a period of the ac field, treating $E_{\vec{K}}$ as a constant value [2,5]. An averaging of the left-hand side does not present any difficulties. Taking into account the inequalities (42) and assuming that $|E_0\cos\psi| \gg E_D, E_M$, we represent first the product of the three factors before $E_{\vec{K}}$ as $i\omega_{\vec{K}}+\gamma_{\vec{K}}$, where

$$\omega_{\vec{K}}=\frac{1}{\tau_d}\frac{E_M}{E_0\cos\psi}, \quad \gamma_{\vec{K}}=\frac{1}{\tau_d}\left(\frac{E_M^2+E_DE_M}{E_0^2\cos^2\psi}+\frac{E_M}{E_q}\right). \quad (44)$$

One sees that $\omega_{\vec{K}}$ is an odd function of E_0 and, consequently, it disappears after the time averaging. The parameter $\gamma_{\vec{K}}$, in contrast, is an even function of E_0; it is not affected by the averaging.

To perform the averaging of the right-hand side of Eq. (39), we should take into account two facts. First, in view of the inequalities $|E_0| \gg E_D, E_M$, the factor $(E_0+iE_D)/(E_M+E_D-iE_0)$ in the leading approximation does not depend on E_0 and equals i. Second, the amplitudes $\vec{A}_{1,2}$ can change considerably when switching $E_0(t)$ because of the changing linear properties of the crystal. This feature has been overlooked in previous studies. As shown in Sec. IV, switching of the applied field transforms $\vec{A}_{1,2}$ into $\vec{A}_{1,2}^*$ if the corresponding input waves are linearly polarized. The average of $\vec{A}_1\cdot\vec{A}_2^*$ in this case is therefore $(\vec{A}_1\cdot\vec{A}_2^*)' \equiv \mathrm{Re}(\vec{A}_1\cdot\vec{A}_2^*)$. Fortunately, the case of linear input polarization is the most important for ac experiments with the sillenites. In what follows we restrict ourselves to this case while considering the wave coupling.

Note that the amplitudes $\vec{A}_{1,2}$ are changing not only because of the linear propagation but also because of diffraction from the light-induced grating. Therefore, it should be verified afterwards that this diffraction does not eliminate the property $\vec{A}_{1,2}(-E_0)=\vec{A}_{1,2}^*(E_0)$ used for the time averaging. We shall do this next in Sec. VII.

Taking into account the results of the averaging, we arrive at the following expression for the steady-state photorefractive response in the presence of a square-wave ac field,

$$E_K=-i|E_0\cos\psi|Q(\vec{A}_1\cdot\vec{A}_2^*)'/I_0, \quad (45)$$

TABLE IV. Characteristic fields for the data of Table III and $\Lambda=20$ μm.

Characteristic fields	BTO	BSO
E_q	250 kV/cm	105 kV/cm
E_M	1.5 kV/cm	0.6 kV/cm
E_D	0.08 kV/cm	0.08 kV/cm

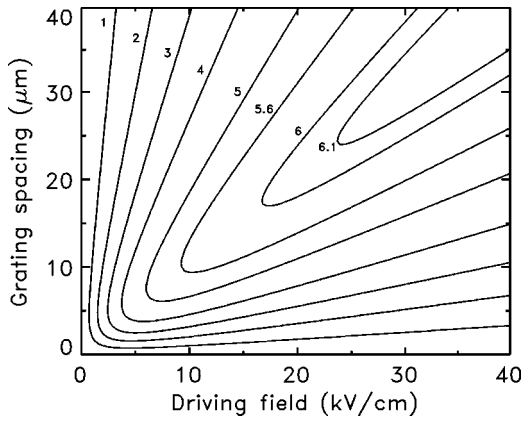

FIG. 7. Dependence of the quality (enhancement) factor Q on the grating spacing Λ and the value of the driving field $|E_0 \cos\psi|$ for $N_t = 2\times10^{16}$ cm^{-3} and $\mu\tau = 2\times10^{-7}$ cm^2/V.

where

$$Q = \frac{|\omega_{\vec{K}}|}{\gamma_{\vec{K}}} = \left(\frac{|E_0 \cos\psi|}{E_q} + \frac{E_D + E_M}{|E_0 \cos\psi|} \right)^{-1}. \tag{46}$$

If $E_q \gg |E_0 \cos\psi| \gg E_M, E_D$, we have $Q \gg 1$. In this important case $\omega_{\vec{K}}$ and $\gamma_{\vec{K}}$ are the eigenfrequency and the damping constant for a space-charge wave with the wave vector $\vec{K}$, and Q is the quality factor for this wave [42]. This factor, as one can see from Eqs. (40) and (46), depends on K and $|E_0 \cos\psi|$.

Equation (45) clearly shows the advantage of the ac technique. The grating remains $\pi/2$ shifted with respect to the light fringes and its amplitude becomes much greater than in the case of zero applied field [2,5]. The enhancement of the grating amplitude is not only due to a large value of $|E_0|$ but also due to a large value of the quality factor, $Q > 1$. Figure 7 shows the dependence of the quality (enhancement) factor Q on $|E_0 \cos\psi|$ and the grating spacing $\Lambda = 2\pi/K$ for the BTO parameters given in Table III. One sees that, for sufficiently large driving field, the optimum grating spacing $\Lambda_{\rm opt} \propto |E_0 \cos\psi|$. For very high values of the driving field, $|E_0 \cos\psi|^2 \gg E_q(E_M + E_D)$, the product $|E_0 \cos\psi|\, Q$ in Eq. (45) saturates at the level of E_q.

Note that large values of the quality (enhancement) factor Q also have some disadvantages for optical applications. The point is that the field of applicability of Eq. (45) is restricted by the inequality $m \lesssim Q^{-2}$, where $m = 2|\vec{A}_1 \cdot \vec{A}_2^*|/I_0$ is the contrast of the light pattern. For larger values of m excitation of higher spatial harmonies, $2\vec{K}, 3\vec{K}, \ldots$, as well as the parametric excitation of spatial subharmonics come onto the scene [42–44]. Both of these effects reduce the amplitude $E_{\vec{K}}$ significantly.

VII. TWO-BEAM COUPLING

A. Equations for two-beam coupling

After we have found the relationships between the grating amplitude $E_{\vec{K}}$ and the light waves amplitudes $\vec{A}_{1,2}$, we can formulate a self-consistent set of equations for two-wave coupling. To simplify this set additionally, we introduce the normalized vectorial amplitudes $\vec{a}_{1,2} = \vec{A}_{1,2}/\sqrt{I_0}$ instead of $\vec{A}_{1,2}$. For these new variables we have the conservation law in the form $|\vec{a}_1|^2 + |\vec{a}_2|^2 = 1$.

In the case of diffusion transport, by combining Eqs. (19) and (43) we have, in steady state,

$$\frac{d\vec{a}_1}{dz} + i\rho\hat{\sigma}_2\vec{a}_1 = \tilde{E}_D(\vec{a}_1 \cdot \vec{a}_2^*)\hat{V}\vec{a}_2,$$
$$\frac{d\vec{a}_2}{dz} + i\rho\hat{\sigma}_2\vec{a}_2 = -\tilde{E}_D(\vec{a}_1^* \cdot \vec{a}_2)\hat{V}\vec{a}_1, \tag{47}$$

where the interaction matrix $\hat{V}$ is given by Eqs. (11).

In the case of a square-wave ac field, using Eqs. (19) and (45) we obtain, for steady-state coupling,

$$\frac{d\vec{a}_1}{dz} - i(\vec{\kappa}\cdot\hat{\vec{\sigma}})\vec{a}_1 = Q|E_0 \cos\psi|(\vec{a}_1 \cdot \vec{a}_2^*)'\hat{V}\vec{a}_2,$$
$$\frac{d\vec{a}_2}{dz} - i(\vec{\kappa}\cdot\hat{\vec{\sigma}})\vec{a}_2 = -Q|E_0 \cos\psi|(\vec{a}_1^* \cdot \vec{a}_2)'\hat{V}\vec{a}_1, \tag{48}$$

where the real vector $\vec{\kappa} = (\kappa_1, \kappa_2, \kappa_3)$ is given by Eqs. (18). Recall that the components $\kappa_{1,3}$ change their sign periodically together with $E_0(t)$, whereas $|\kappa_{1,3}|, |E_0|$, and $\kappa_2 = -\rho$ remain constant.

Let us underline the difference between the conditions of applicability of Eqs. (47) and (48). The first set of equations is valid for arbitrary input polarizations of the waves 1 and 2 and, actually, without any severe restrictions on the contrast $m = 2|\vec{a}_1 \cdot \vec{a}_2^*|$. The nonlinear effects are, however, fairly weak in the diffusion case. Equations (48) pretend to be valid only for linear input polarizations and for the contrast $2|\vec{a}_1 \cdot \vec{a}_2^*| \lesssim 1/Q^2$. To justify fully these equations we should verify (see the previous section) that $\vec{a}_{1,2} \to \vec{a}_{1,2}^*$ when $E_0 \to -E_0$. Taking into account that the matrix $\hat{V}$ does not depend on E_0 and that $\kappa_{1,3} \propto E_0$, one can make sure that the necessary transformation property is really in harmony with the structure of Eqs. (48).

Using Eqs. (48) and the general properties of the $\hat{V}$ matrix formulated in subsection 2B one can check that the scalar product $(\vec{a}_1 \cdot \vec{a}_2^*)$, which is supposed to be real at input, remains real for any z. Therefore, the prime in Eqs. (48) can be omitted. One should not forget, however, that Eqs. (48) cannot be applied to the case of elliptic input polarizations.

Neither of the vectorial equations (47) and (48) can be solved analytically in the general case, in contrast with the case of scalar two-wave coupling. For many important limiting cases, however, analytical solutions to the vectorial two-wave problem are possible. The character of the approximations applicable to Eqs. (47) and (48) is quite different.

As one can see from Tables I and III, and Eqs. (11), the rotatory power ρ is typically significantly greater than the elements of the matrix $\tilde{E}_D\hat{V}$. This is especially true for BSO (and also BGO) crystals. Therefore, we can exploit the in-

equality $\tilde{E}_D|V_{ij}/\rho| \ll 1$ in solving Eqs. (47). Another inequality relevant to experiment is $E_D|\hat{V}|l \ll 1$; this means that the crystal is nonlinearly thin.

For the ac case, the inequality $Q|E_0 \cos\psi\hat{V}| \gg |\rho|$ is often fulfilled. It is the basis for perturbative procedures to solve Eqs. (48).

B. Diffusion case

1. Approximation of a nonlinearly thin crystal

To exploit the inequality $|\hat{V}|E_D l \ll 1$, we first exclude the linear terms responsible for the optical activity from Eqs. (47). This may be done by the following linear transformation from $\vec{a}_{1,2}$ to new amplitudes $\vec{b}_{1,2}$,

$$\vec{b}_{1,2}(z) = e^{i\rho z\hat{\sigma}_2}\vec{a}_{1,2}(z). \tag{49}$$

Actually, this is analogous to the so-called interaction representation in quantum mechanics [35,36]. The introduced transformation is unitary, i.e., it does not change the scalar products; in particular, $\vec{b}_1^* \cdot \vec{b}_2 \equiv \vec{a}_1^* \cdot \vec{a}_2$. Furthermore, it does not change the boundary conditions because $\vec{b}_{1,2}(0) = \vec{a}_{1,2}(0)$. Using Eqs. (13), (14), and (17), we have instead of Eqs. (47),

$$\begin{aligned} \frac{d\vec{b}_1}{dz} &= \tilde{E}_D(\vec{b}_1 \cdot \vec{b}_2^*)\hat{h}\vec{b}_2, \\ \frac{d\vec{b}_2}{dz} &= -\tilde{E}_D(\vec{b}_1^* \cdot \vec{b}_2)\hat{h}\vec{b}_1, \end{aligned} \tag{50}$$

with $\hat{h} = \hat{h}(z)$ given by

$$\hat{h} = \nu_0\hat{1} + \cos 2\rho z(\vec{\nu}\cdot\hat{\vec{\sigma}}) - \sin 2\rho z(\nu_3\hat{\sigma}_1 - \nu_1\hat{\sigma}_3). \tag{51}$$

Within the first order perturbation theory, we obtain from Eqs. (50) the expressions for $\delta\vec{b}_{1,2} = \vec{b}_{1,2}(l) - \vec{b}_{1,2}(0)$,

$$\begin{aligned} \delta\vec{b}_1 &= \tilde{E}_D(\vec{a}_1 \cdot \vec{a}_2^*)\left[\nu_0 l + \frac{\sin 2\rho l}{2\rho}(\vec{\nu}\cdot\hat{\vec{\sigma}}) - \frac{\sin^2\rho l}{\rho}(\nu_3\hat{\sigma}_1 - \nu_1\hat{\sigma}_3)\right]\vec{a}_2, \\ \delta\vec{b}_2 &= -\tilde{E}_D(\vec{a}_1^* \cdot \vec{a}_2)\left[\nu_0 l + \frac{\sin 2\rho l}{2\rho}(\vec{\nu}\cdot\hat{\vec{\sigma}}) - \frac{\sin^2\rho l}{\rho}(\nu_3\hat{\sigma}_1 - \nu_1\hat{\sigma}_3)\right]\vec{a}_1. \end{aligned} \tag{52}$$

The amplitudes $\vec{a}_{1,2}$ on the right-hand side of Eqs. (52) are supposed to be taken at $z=0$. The smallness of the corrections, $|\delta\vec{b}_{1,2}| \ll |\vec{a}_{1,2}|$, is guaranteed by the smallness of the products $\tilde{E}_D\nu l$ and $\tilde{E}_D\nu_0 l$, irrespective of the value of ρl.

From Eqs. (52) we can calculate further the changes in the wave intensities,

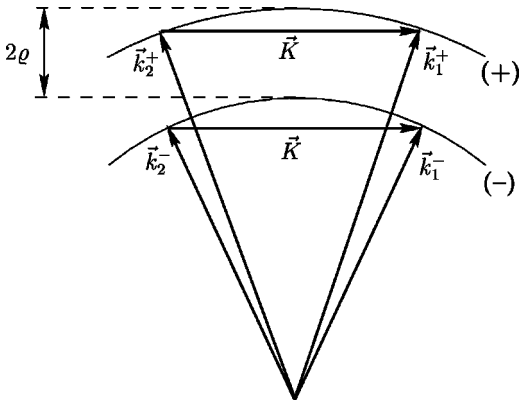

FIG. 8. Geometrical scheme of wave coupling for weak photorefractive nonlinearity.

$$\delta|\vec{a}_{1,2}|^2 = \pm\tilde{E}_D(\vec{a}_1 \cdot \vec{a}_2^*)\left[\vec{a}_1^* \cdot \left(\nu_0 l + \frac{\sin 2\rho l}{2\rho}(\vec{\nu}\cdot\hat{\vec{\sigma}}) - \frac{\sin^2\rho l}{\rho}(\nu_3\hat{\sigma}_1 - \nu_1\hat{\sigma}_3)\right)\vec{a}_2\right] + \text{c.c.} \tag{53}$$

This expression is valid for arbitrary input polarizations and intensity ratio. Usually in 2W-mixing experiments the input polarizations are linear and equal for waves 1 and 2. In this case the polarization state is defined by the angle φ between the polarization plane and the x axis and Eq. (53) attains the form

$$\delta|\vec{a}_{1,2}|^2 = \pm\frac{m^2\tilde{E}_D}{2}\left[\nu_0 l + \frac{\sin 2\rho l}{2\rho}(\nu_3\cos 2\varphi + \nu_1\sin 2\varphi) - \frac{\sin^2\rho l}{\rho}(\nu_3\sin 2\varphi - \nu_1\cos 2\varphi)\right], \tag{54}$$

where m is the input value of the contrast. This expression is useful for the diagnosis of different crystals taking into account the photoelastic contributions to ν_0 and $\vec{\nu}$. It explicitly shows the effect of the optical activity and of the initial polarization on the photorefractive gain.

The grating amplitude $E_{\vec{K}}$ remains nearly constant within the above approximation, irrespective of the value of the product ρl. This constant amplitude is given by Eq. (43) with the input values of the amplitudes $\vec{A}_{1,2}$. The diffraction efficiency of such a grating is described by the formulas of Sec. V. Measurements of the diffraction efficiency may be performed by the instantaneous blocking of one of the pump beams or with the use of auxiliary Bragg-matched readout beams.

2. Resonant approximation

In the case when the crystal is not nonlinearly thin and, additionally, $|\rho| \gg E_D|\hat{V}|$, one can use another approximation based on the introduction of the scalar amplitudes of the optical $(\pm)$ modes. We explain the idea of this approximation, which may be called resonant, with the help of Fig. 8. The distance between the wave surfaces, 2ρ, is much greater than the broadening of these surfaces owing to the wave coupling. Furthermore, spatial gratings may be recorded only

by wave pairs of the same polarization (+ or −) because wave pairs with orthogonal polarizations produce no intensity modulation. For this reason, diffraction processes which change the polarization state are nonresonant (off-Bragg) and may be neglected.

To perform the resonant approximation, we introduce the scalar amplitudes $a_\pm$ (for the moment we omit the subscripts 1,2) by means of

$$\vec{a}=a_+\vec{e}_+e^{i\rho z}+a_-\vec{e}_-e^{-i\rho z} \tag{55}$$

where, in agreement with Eqs. (27), the unit polarization vectors are $\vec{e}_\pm=(1,\pm i)/\sqrt{2}$. By multiplying Eqs. (47) scalarly by $\vec{e}_\pm^{\,*}$ and omitting quickly oscillating [as $\exp(2i\rho z)$] nonresonant terms which appear on the right-hand sides, we obtain

$$\begin{aligned}\frac{da_{1\pm}}{dz}&=\tilde{E}_D\nu_0(a_{1+}a_{2+}^*+a_{1-}a_{2-}^*)a_{2\pm},\\ \frac{da_{2\pm}}{dz}&=-\tilde{E}_D\nu_0(a_{1+}^*a_{2+}+a_{1-}^*a_{2-})a_{1\pm}.\end{aligned} \tag{56}$$

This compact system of four coupled equations corresponds to the scheme of wave coupling discussed above. It possesses the following integrals (conservation laws):

$$\begin{aligned}|a_{1+}|^2+|a_{2+}|^2&=I_1,\\ |a_{1-}|^2+|a_{2-}|^2&=I_2,\\ a_{1+}a_{2-}-a_{2+}a_{1-}&=J_1,\\ a_{1+}a_{1-}^*+a_{2+}a_{2-}^*&=J_2.\end{aligned} \tag{57}$$

$I_{1,2}$ are real and $J_{1,2}$ are complex constants. Consequently, the set of four complex equations (56) has, in fact, only two degrees of freedom. It is analogous to the equations for the scalar 4W coupling and, in many cases, admits analytical solutions [45]. In the case when two incident waves have the same polarizations it is reduced to equations for the scalar two-wave coupling. The fractions of the (+) and (−) eigenmodes in each of the beams 1 and 2 here remain unchanged along the crystal.

Unfortunately, strong nonlinear effects can hardly be attained in the sillenites in the diffusion case in view of fairly small values of the product $s\tilde{E}_D$.

C. Ac case

In this case, beam coupling is very strong and the approximation of a nonlinearly thin crystal usually fails. On the other hand, the characteristic nonlinear rate here, $sQ|E_0|$, is comparable with (or even larger than) the distance between the wave surfaces, 2κ. In this situation the resonant approximation also fails. The most useful analytical tool here is the undepleted pump approximation. It is valid when the intensity of one beam (let it be beam 1) remains weak throughout the crystal, i.e., the contrast m remains small. This approximation is applicable to describe the weak signal amplification, as well as the light-induced scattering (the fanning phenomenon). Note that the case of an undepleted pump is often the only one that can be considered on the basis of Eqs. (48) because of the restriction $2|\vec{a}_1\cdot\vec{a}_2^*|\lesssim Q^{-2}$ on the contrast.

To exploit the undepleted pump approximation, it is useful to get rid of the linear terms in Eqs. (48) responsible for the linear propagation. This may be done by the unitary transformation

$$\vec{a}_{1,2}=e^{i(\vec{\kappa}\cdot\hat{\vec{\sigma}})z}\vec{b}_{1,2} \tag{58}$$

to new amplitudes $\vec{b}_{1,2}$, which is analogous to the one performed in the previous subsection. Within the new representation Eqs. (48) attain the form

$$\begin{aligned}\frac{d\vec{b}_1}{dz}&=(\vec{b}_1\cdot\vec{b}_2^*)'(q_0+\vec{q}\cdot\hat{\vec{\sigma}})\vec{b}_2,\\ \frac{d\vec{b}_2}{dz}&=-(\vec{b}_1\cdot\vec{b}_2^*)'(q_0+\vec{q}\cdot\hat{\vec{\sigma}})\vec{b}_1,\end{aligned} \tag{59}$$

where $q_0=Q\,|E_0\cos\psi|\nu_0$ is a real constant,

$$\begin{aligned}\vec{q}=Q\,|E_0\cos\psi|\,&(\vec{o}(\vec{\nu}\cdot\vec{o})+[\vec{\nu}-\vec{o}(\vec{\nu}\cdot\vec{o})]\cos 2\kappa z\\ &-(\vec{\nu}\vec{o})\sin 2\kappa z)\end{aligned} \tag{60}$$

is a real 3D vector dependent on the propagation coordinate, and, as above, $\vec{o}=\vec{\kappa}/\kappa$.

The derivative $d\vec{b}_2/dz$, being of the second order in $\vec{b}_1$, may be put equal to zero. Therefore in the first equation of Eqs. (59) we can put $\vec{b}_2(z)=\vec{b}_2(0)=\vec{a}_2(0)$. Since the amplitudes $\vec{a}_{1,2}$ are normalized to unity and $|\vec{a}_2|^2\gg|\vec{a}_1|^2$, we have $|\vec{a}_2|^2\simeq 1$. Now we recall that the initial Eqs. (48) are valid only for linearly polarized input waves. This means that the input amplitude $\vec{a}_2(0)$ is a real unit polarization vector; it may be specified by the angle φ_2 measured from the x axis, $\vec{a}_2(0)=(\cos\varphi_2,\sin\varphi_2)$.

Multiplying the equation for $\vec{b}_1$ scalarly by $\vec{b}_2$, we arrive at the following scalar equation for $\vec{b}_1\cdot\vec{b}_2$,

$$\frac{d}{dz}(\vec{b}_1\cdot\vec{b}_2)=(\vec{b}_1\cdot\vec{b}_2)'(q_0+q_1\sin 2\varphi_2+q_3\cos 2\varphi_2). \tag{61}$$

In accordance with Eq. (60), the components $q_{1,3}$ are real functions of z. The imaginary part of the product $\vec{b}_1\cdot\vec{b}_2$ therefore remains equal to zero. This does not mean, however, that the vector $\vec{b}_1(z)$ is real; in general it is complex, i.e., the output polarization of wave 1 is elliptic. Another important feature of Eq. (61) is that the values $q_{0,1,3}$ remain unchanged during switching of the applied field; this means, in turn, that the product $\vec{b}_1\cdot\vec{b}_2$ does not experience any changes because of switching.

By integrating Eq. (61), using Eqs. (18), and recalling that $\vec{b}_1\cdot\vec{b}_2=\vec{a}_1\cdot\vec{a}_2$, we obtain the following explicit relation,

$$(\vec{a}_1\cdot\vec{a}_2)(z)=(\vec{a}_1\cdot\vec{a}_2)(0)\exp(\Gamma z+C_1\sin 2\kappa z+C_2\sin^2\kappa z), \tag{62}$$

where

$$\Gamma = Q|E_0 \cos\psi|\left[\nu_0 + \frac{(\vec{\nu}\cdot\vec{\kappa})}{\kappa^2}(\kappa_1 \sin 2\varphi_2 + \kappa_3 \cos 2\varphi_2)\right] \tag{63}$$

and

$$\begin{aligned} C_1 &= \frac{Q|E_0 \cos\psi|}{2\kappa^3}([\kappa^2\nu_1 - \kappa_1(\vec{\nu}\cdot\vec{\kappa})]\sin 2\varphi_2 + [\kappa^2\nu_3 \\ &\quad - \kappa_3(\vec{\nu}\cdot\vec{\kappa})]\cos 2\varphi_2), \\ C_2 &= -\frac{Q|E_0 \cos\psi|\rho}{\kappa^2}(\nu_3 \sin 2\varphi_2 - \nu_1 \cos 2\varphi_2). \end{aligned} \tag{64}$$

We see from Eq. (62) that the parameter Γ, which we call the increment, primarily defines the process of spatial growth. For $\Gamma l \gg 1$, the theory predicts a very strong amplification of the weak wave 1.

A few general features of the expression (63) for the increment are worth noting.

(i) Γ consists of an isotropic and an anisotropic contribution. The isotropic contribution ($\propto \nu_0$) does not depend on the polarization of the pump, whereas the anisotropic one ($\propto \vec{\nu}\cdot\vec{\kappa}$) depends essentially on this angle; in particular, it changes the sign when $\varphi_2 \to \varphi_2 \pm \pi/2$.

(ii) The opposite directions of the grating vector correspond to the opposite signs of the increment, i.e., $\Gamma \to -\Gamma$ when $\vec{K} \to -\vec{K}(\zeta \to \zeta \pm \pi)$. This feature is clearly seen from Eqs. (18), (20), and (22).

(iii) The increment Γ does not depend on the sign of E_0 and $\vec{n}^0$. This follows from the definition of the vector $\vec{\kappa}$ [see Eqs. (18)].

(iv) Since Γ is odd in ν_0, $\vec{\nu}$ and even in $\vec{\kappa}$, the transition from the basic configuration shown in Fig. 1(a) to the nonequivalent configuration of Fig. 1(b) results in the replacement $\Gamma(\zeta, \zeta_0) \to -\Gamma(\zeta, \zeta_0)$.

The contributions to the exponent of Eq. (62) related to the parameters $C_{1,2}$ influence the spatial amplification significantly only for $|C_{1,2}| \gtrsim 1$. As seen from Eqs. (64), each of the parameters $C_{1,2}$ is the product of the enhancement factor Q, which typically does not exceed 5–6 [46], and a dimensionless factor dependent on the optical configuration in question and on the polarization angle φ_2. For many important cases the dimensionless factors, $C_{1,2}/Q$, are much less than one. For example, we have $|C_2|/Q \ll 1$ for two limiting cases, $|sE_0| \gg |\rho|$ and $|sE_0| \ll |\rho|$; the first case is relevant to ac experiments with BTO crystals and the second one may often be justified for BSO and BGO crystals. The factor $|C_1|/Q$ is small for $|\rho| \gg |sE_0|$; in the opposite limit, $|\rho| \ll |sE_0|$, it is definitely small for $\vec{K} \| \vec{E}_0$ because of the smallness of the elasto-optic contributions to $\nu_{1,3}$ (see also the next section).

An important feature of Eq. (62) is that the argument of the exponent does not depend on the polarization of the weak wave 1; it depends, however, on the pump polarization angle φ_2. The dependence on the input polarization of wave 1 is only expressed by the preexponential factor, $(\vec{a}_1 \cdot \vec{a}_2)(0)$. The mentioned properties enable us to optimize the polarization angles for the case of strong amplification $|a_1(l)| \gg |a_1(0)|$. First, we should set $\vec{a}_1(0) \| \vec{a}_2(0)$ to maximize the preexponent. Second, which is more important, we should optimize the increment Γ with respect to φ_2. At the optimum we have

$$\Gamma = Q|E_0 \cos\psi|\left[\nu_0 + \frac{\sqrt{\kappa_1^2 + \kappa_3^2}|\vec{\nu}\cdot\vec{\kappa}|}{\kappa_1^2 + \kappa_3^2 + \rho^2}\right],$$

$$\sin 2\varphi_2 = \frac{\kappa_1 \operatorname{sign}(\vec{\nu}\cdot\vec{\kappa})}{\sqrt{\kappa_1^2 + \kappa_3^2}}, \quad \cos 2\varphi_2 = \frac{\kappa_3 \operatorname{sign}(\vec{\nu}\cdot\vec{\kappa})}{\sqrt{\kappa_1^2 + \kappa_3^2}} \tag{65}$$

and, correspondingly,

$$\vec{a}_1(l) \cdot \vec{a}_2 \approx |\vec{a}_1(0)| e^{\Gamma l}. \tag{66}$$

Note that the optimum polarization angle φ_2 does not depend on the sign of E_0.

The expression (65) for Γ may further be maximized with respect to the length of the grating vector, K, and to the angles ζ and ζ_0, specifying the orientations of $\vec{K}$ and $\vec{E}_0$. Such a maximization is important for practical purposes. An example of the maximization of the increment as applied to BTO crystals is given in the next section. As a general assertion we can say that the absolute maximum of $\Gamma(\zeta, \zeta_0, K)$ indeed corresponds to $\vec{K} \| \vec{E}_0$ (to $\psi \equiv \zeta - \zeta_0 = 0$) and to the length K maximizing the enhancement factor $Q(|E_0|, K)$ for a given value of E_0 (see Fig. 7). For an arbitrary angle ζ_0 the maximum of $\Gamma(\zeta)$ generally takes place for $\psi \neq 0$.

The output value of the product $\vec{a}_1 \cdot \vec{a}_2$ is definitely an important measurable characteristic of the spatial amplification. However, it does not fully describe the output properties of wave 1 because it cannot specify its output intensity and polarization. To find the output value of the vectorial amplitude $\vec{b}_1$ we should substitute the value of the product $\vec{b}_1 \cdot \vec{b}_2^* = \vec{a}_1 \cdot \vec{a}_2$, given by Eq. (62), into the first of Eqs. (59) and calculate the integral. In the case when $|C_{1,2}| \gtrsim 1$, the analytical calculation is problematic and the polarization properties of the amplified wave are rather complicated. Fairly simple results may be obtained for $\vec{K} \| \vec{E}_0$ and $|\rho| \ll |sE_0|$, which are relevant to ac experiments with BTO crystals.

In the limit under study, which corresponds to $\vec{\nu} \| \vec{\kappa}$, we put $\vec{q} = Q|E_0|\vec{\nu}$, $C_{1,2} = 0$ and $\Gamma = Q|E_0|(\nu_0 + \nu_1 \sin 2\varphi_2 + \nu_3 \cos 2\varphi_2)$. Assuming that $\exp(\Gamma l) \gg 1$, we obtain from Eqs. (59) and (62), for the vector $\vec{b}_1(l)$,

$$\vec{b}_1(l) \simeq (\vec{b}_1 \cdot \vec{b}_2)(0) e^{\Gamma l} \frac{Q|E_0|}{\Gamma}(\nu_0 + \vec{\nu}\cdot\hat{\vec{\sigma}})\vec{b}_2. \tag{67}$$

This expression allows one to calculate the gain factor for the intensity, $|\vec{a}_1(l)/a_1(0)|^2 \equiv |\vec{b}_1(l)/b_1(0)|^2$. It is obviously given by $\exp(2\Gamma l)$ with a preexponential factor (of the order of 1) depending on the input polarization vectors. The optimum direction of $\vec{b}_{1,2}(0)$ coincides with the direction of the eigenvector of the matrix $\vec{\nu}\cdot\hat{\vec{\sigma}}$, which corresponds to the large eigenvalue ν. The corresponding inclination angle φ_2

and the increment Γ are given by $\cos 2\varphi_2=\nu_3/\nu$, $\sin 2\varphi_2=\nu_1/\nu$, and $\Gamma=Q|E_0|(\nu_0+\nu)$. With these values we have

$$|\vec{a}_1(l)/a_1(0)|^2=e^{2Q|E_0|(\nu_0+\nu)l}. \tag{68}$$

To describe the output polarization state we should return from $\vec{b}_1(l)$ to the amplitude $\vec{a}_1(l)$ using Eq. (58). In the case of arbitrary linear polarizations of waves 1 and 2, the output wave 1 is elliptically polarized. For the above optimum conditions the output polarization state coincides, however, with the input one.

VIII. APPLICATIONS TO BTO CRYSTALS

Most of the factual data on strong 2W mixing are obtained in ac experiments with fiberlike BTO crystals. The amplitude of the square-wave applied field ranges here from 20 to 50 kV/cm and the input pump beams are linearly polarized. Below we apply the results of the previous subsection VII C to a description of 2W mixing in BTO crystals and to an interpretation of the available experimental data. In our subsequent treatment we do not suppose that $\vec{K}\|\vec{E}_0$.

A. Characteristic features of BTO crystals

Let us make some numerical estimates to define the characteristic features of the ac case as applied to BTO crystals. Using the data of Table I and setting $|E_0|=30$ kV/cm, we have $|sE_0|\simeq 12\ \text{cm}^{-1}$. This value considerably exceeds the rotatory power $\rho\simeq 6.5$ deg/mm$\simeq 1.13\ \text{cm}^{-1}$. Consequently, we have $\kappa_1^2+\kappa_3^2\gg\kappa_2^2\equiv\rho^2$; this means that the effect of the optical activity on Γ and $C_{1,2}$ [see Eqs. (63) and (64)] may be neglected.

Figure 7 shows that the maximum value of $Q(\Lambda)$ saturates at the level $Q\simeq 6$ for $|E_0\cos\psi|\gtrsim 15$ kV/cm. This immediately gives a rough estimate $\Gamma\approx 70\ \text{cm}^{-1}$ for the increment. Such a high value means the possibility of a very strong spatial amplification of proper light waves.

As seen from Fig. 7, the optimum grating spacing Λ is directly proportional to the absolute value of the driving field $|E_0\cos\psi|$. For $|E_0\cos\psi|=30$ kV/cm we have $\Lambda_{opt}\simeq 30\ \mu$m, which corresponds to the interaction angle θ (taken in air) of about 1.2°. Such small values of the characteristic angles justify the used paraxial approximation with a large margin of safety.

Using the results of subsection VII C and neglecting optical activity, we can find the optimum configuration for 2W coupling in BTO crystals. By setting $\zeta=\zeta_0(\psi=0)$, $\Lambda=\Lambda_{opt}$, and $\rho=0$ in Eq. (65), and recalling the definition of $\kappa_{1,3}$ and $\nu_{0,1,3}$, we obtain, for the increment Γ as a function of ζ_0,

$$\Gamma=s|E_0|Q_{\max}(|E_0|)f(\zeta_0), \tag{69}$$

$$f=0.5(H_{xx}+H_{yy})+|\sin\zeta_0 H_{xy}-0.25\cos\zeta_0(H_{xx}-H_{yy})|/\sqrt{\sin^2\zeta_0+0.25\cos^2\zeta_0}.$$

Figure 9 shows the dependence $f(\zeta_0)$ calculated for the data of Fig. 2(a) for $H_{ij}(\zeta_0)$. With the elasto-optic contributions omitted (the dashed line) we have the maximum value $f_{\max}=(\sqrt{3}+1/\sqrt{3})/2\simeq 1.155$ for $\zeta_0=\arccos(1/\sqrt{3})\simeq 54.7°$,

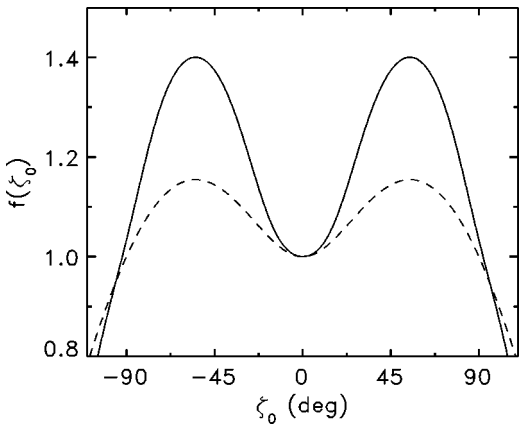

FIG. 9. Dependence $f(\zeta_0)$ for BTO crystals; the dashed line is plotted with neglected elasto-optic contributions.

which corresponds to the diagonal configuration. This result coincides with the prediction made in Ref. [25]. Note that we have $f=1$ for both the longitudinal ($\zeta_0=0$) and transversal ($\zeta_0=\pi/2$) configurations; this means that the gain in $\Gamma(\zeta_0)$ attained for the diagonal geometry is quite moderate (about 15%). With the elasto-optic contributions taken into account (the solid line), the function $f(\zeta_0)$ peaks again at $\zeta_0\simeq 54.7°$; here we have $f_{\max}\simeq 1.4$. Therefore, the gain in the increment for the diagonal geometry becomes as high as 40% in comparison with the longitudinal and transversal geometries. The absolute maximum of the increment for BTO crystals and $E_0=30$ kV/cm may be evaluated as $\Gamma_{\max}\simeq 100\ \text{cm}^{-1}$.

Now we estimate the effect of the parameters $C_{1,2}$ in Eq. (62) on the spatial amplification in BTO crystals. Using Eqs. (64), the inequality $|\rho|\ll|sE_0|$, and neglecting the elasto-optic contributions, one can find that $|C_2|\lesssim Q|\cos\psi\rho/sE_0|$; for $Q\simeq 6$ and $|\rho/sE_0|=0.1$ it gives $|C_2|\lesssim 0.6$. In other words, the effect of the parameter C_2 is fairly small. For the parameter C_1 we have within the same approximation,

$$C_1\simeq\frac{Q}{8}|\cos\psi|\sin\psi\frac{(\cos\zeta_0\sin 2\varphi_2+2\sin\zeta_0\cos 2\varphi_2)}{(\sin^2\zeta_0+0.25\cos^2\zeta_0)^{3/2}}. \tag{70}$$

This expression shows that the maximum effect of C_1 takes place for $|\sin 2\psi|\approx 1$, i.e., for large angles between $\vec{K}$ and $\vec{E}_0$. This case is not actually relevant for the amplification of weak signals but it is important for the description of light-induced scattering. Furthermore, one can find that $|C_1|\lesssim Q|\sin 2\psi|/8$ for the transversal and diagonal configurations irrespective of the polarizaton angle φ_2. This means that the spatial oscillations in Eq. (62) related to C_1 are of minor importance as compared with the strong exponential growth with the rate Γ. For the longitudinal configuration ($\zeta_0=0$) and $\varphi_2=\pi/4$ we have the maximum value, $C_1\simeq Q\sin 2\psi/2$; it may be practically as high as (2–3). The effect of the spatial oscillations superposed on the exponential spatial growth is pronounced in this case. Below we shall use Eq. (70) and the above estimates as applied to particular cases.

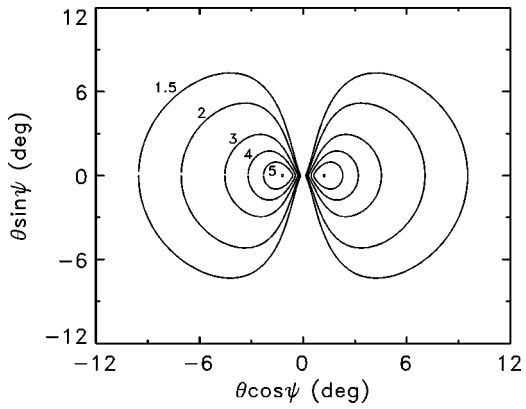

FIG. 10. Contour lines of the product $Q(\lambda\vec{K}/2\pi)|\cos\psi|$ for $|E_0|=30$ kV/cm. The chosen parameters of the BTO crystals are the same as for Fig. 7.

B. General observations on the angular dependence of the increment

Our next aim is to describe the dependence of the increment Γ on the propagation direction of a weak light beam and on the polarization of the pump beam as applied to the experimental conditions. To attain this goal, it is convenient to use the polar interaction angle $\theta=\lambda|\vec{K}|/2\pi$ instead of $|\vec{K}|$ and to measure all of the azimuth angles not from the x axis but from the horizontal parallel to the applied field; this means that, instead of the angles ζ and φ_2 (see Fig. 4), we use the angles $\psi=\zeta-\zeta_0$ and $\varphi_p=\varphi_2-\zeta_0$.

As is seen from Eq. (63), the angular dependence of the increment originates from two different sources, namely, from the product $Q|\cos\psi|$ and from the square bracket. The quality factor Q [see Eq. (46)], depends on θ and ψ. It is remarkable that the function $Q(\theta,\psi)$ has nothing to do with the choice of the optical configuration; it is defined by the material parameters and the amplitude $|E_0|$. Figure 10 shows the angular dependence of $Q|\cos\psi|$ for the representative parameters of BTO given in Tables I and III, and $|E_0|=30$ kV/cm. It is clearly seen that this dependence is symmetric about the horizontal and the vertical directions, and it is characterized by two pronounced maximums. Note that an increase of $|E_0|$ does not give any real gain in the maximum enhancement factor starting from ≈ 10 kV/cm; in harmony with Fig. 7 it results mainly in a decrease of the optimum interaction angle θ. The second factor [the square bracket in Eq. (63)] does not depend on the polar angle θ; its dependence on ψ and φ_p is defined by the optical configuration in question. After the above preliminaries we turn to the treatment of particular optical configurations that correspond to different values of the angle ζ_0 in Fig. 1(a).

C. Longitudinal configuration, $\vec{E}_0\|[001]$

In this simplest case we put $\zeta_0=0,\psi=\zeta,\varphi_p=\varphi_2$, and $\kappa_1=0$. Using Eqs. (18) and (63), we obtain

$$\Gamma=s|E_0\cos\psi|Q(H_{xx}\cos^2\varphi_p+H_{yy}\sin^2\varphi_p). \qquad (71)$$

The dependences $H_{xx}(\zeta),H_{yy}(\zeta)$ are given in Fig. 2. If the elasto-optic contribution is omitted, Eq. (71) simplifies to

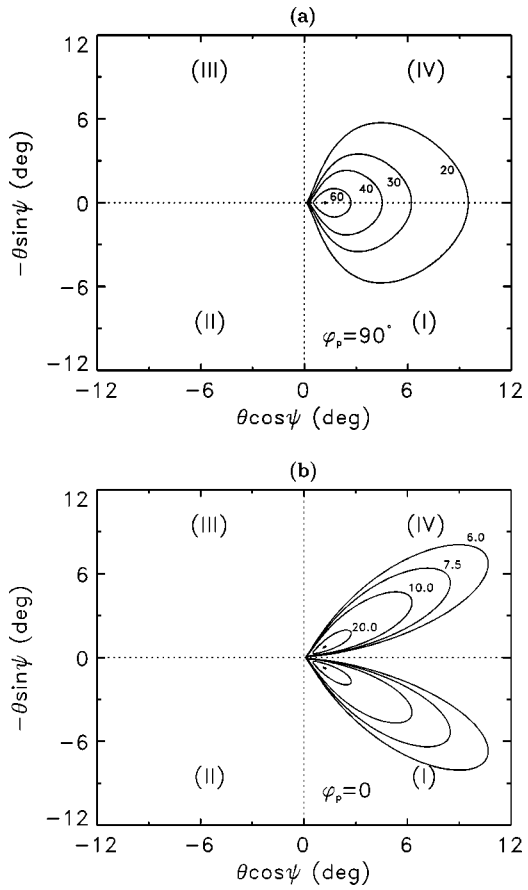

FIG. 11. Contour lines of the increment $\Gamma(\lambda\vec{K}/2\pi)=\text{const}>0$ for the longitudinal configuration; the cases (a) and (b) correspond to the vertical ($\varphi_p=\pi/2$) and horizontal ($\varphi_p=0$) polarizations of the pump wave 2.

$$\Gamma=s|E_0\cos\psi|Q\sin^2\varphi_p\cos\psi. \qquad (72)$$

In accordance with this expression, the optimum polarization angle is $\varphi_p=\pi/2$ (the vertical polarization) and the dependence on the azimuth angle ψ is characterized by a maximum at $\psi=0$ and by a minimum at $\psi=\pi$. For $\varphi_p=0$ (the horizontal polarization) we have $\Gamma=0$, which is no exponential amplification.

Figures 11(a) and 11(b) show the dependences $\Gamma(\theta,\psi)$ plotted for $\varphi_p=\pi/2$ and 0, respectively, on the basis of Eq. (71). In the first case, taking into account the elasto-optic effect does not produce any substantional changes as compared with the result given by Eq. (72); the maximum value of Γ here is about 75 cm^{-1}. For $\varphi_p=0$ the elasto-optic effect removes the prohibition on wave coupling; for $\psi\neq 0$ the increment Γ takes positive but relatively small values. Note finally that the parameter C_1 given by Eq. (70) turns to zero for $\varphi_p=\pi/2$ and 0.

The dependence $\Gamma(\theta,\psi)$ for the backward configuration obtained by a 180° rotation of the sample around the vertical [110] axis (see Fig. 4), may be obtained by a 180° rotation of the spatial distributions shown in Fig. 11 around the vertical axis. This follows from the general observation of Sec. III that the characteristics of 2W coupling remain the same for any backward configuration, provided that all of the angles are measured from the corresponding principal axis.

D. Transversal configuration, $\vec{E}_0 \perp [001]$

In this case we set $\zeta_0=\pi/2$, $\zeta=\psi+\pi/2$, $\varphi_2=\varphi_p+\pi/2$ and, correspondingly, $\kappa_1=sE_0$, $\kappa_3=0$. Using Eq. (63) we get

$$\Gamma = s|E_0 \cos\psi| Q(\nu_0 - \nu_1 \sin 2\varphi_p), \tag{73}$$

where $\nu_{0,1}$ are given by Eqs. (18) and Fig. 3. With neglected elasto-optic contributions we obtain, instead of Eq. (73),

$$\Gamma = -\frac{1}{2} s|E_0 \cos\psi| Q(\sin\psi + 2\cos\psi \sin 2\varphi_p). \tag{74}$$

For $\varphi_p=0,\pi/2$ the above expressions for Γ yield two symmetric lobes in quadrants III and IV [see Fig. 12(a)]. The optimum conditions for the spatial amplification correspond to $\varphi_p=\pm\pi/4$ and $\psi=-0.5\pi\mp\arccos(2/\sqrt{5})\simeq(-90\mp64)°$ see Figs. 12(b) and 12(c). The parameter C_1 is zero in this particular case. A 180° rotation of the sample around the vertical [001] axis here does not change the angular dependence $\Gamma(\theta,\psi)$ because the forward and backward configurations are physically equivalent.

E. Diagonal configurations

Let us first consider the diagonal configuration, $\vec{E}_0 \| [\overline{1}11]$. In this case we have [see also Fig. 4(a)] $\zeta=\psi+\zeta_0$, $\varphi_2=\varphi_p+\zeta_0$ with $\zeta_0=\arctan(\sqrt{2})\simeq54.7°$ and, correspondingly, $\kappa_1=\sqrt{2}sE_0/\sqrt{3}$, $\kappa_3=-sE_0/2\sqrt{3}$. Using Eq. (63) we obtain, after simple calculations,

$$\Gamma_{[\overline{1}11]} = \frac{1}{3}|E_0 \cos\psi| Q[3\nu_0 + (2\sqrt{2}\nu_1 - \nu_3)\cos 2\varphi_p]. \tag{75}$$

With neglected elasto-optic contributions to $\nu_{0,1,3}(\zeta)$ this relation is replaced by

$$\Gamma_{[\overline{1}11]} = \frac{1}{2\sqrt{3}} s|E_0 \cos\psi| Q[(\cos\psi - \sqrt{2}\sin\psi) + (3\cos\psi + \sqrt{2}\sin\psi)\cos 2\varphi_p]. \tag{76}$$

For $\varphi_p=0$ (the horizontal polarization) the increment $\Gamma_{[\overline{1}11]}$ as a function of ψ peaks at $\psi=0$; here, $\Gamma_{[\overline{1}11]}=2s|E_0|Q/\sqrt{3}$. This case is optimum for the spatial amplification.

Figure 13(a) shows the dependence $\Gamma_{[\overline{1}11]}(\theta,\psi)$ obtained for $\varphi_p=0$ from Eq. (75). It gives qualitatively the same result as the simplified Eq. (76). The angular distribution here has the form of a lobe pointed in the horizontal direction. The absolute maximum of the increment, $\Gamma_{[\overline{1}11]}\simeq100\ \mathrm{cm}^{-1}$, is attained just in this case.

For $\varphi_p=\pm\pi/2$ (the vertical polarization) the square bracket in Eq. (76) peaks at $\psi=\arctan(\sqrt{2})-\pi\simeq-125.3°$. Since the product $Q|\cos\psi|$ decreases gradually with increasing $|\sin\psi|$, the maximum of $\Gamma(\psi)$ shifts slightly from $\psi=-125.3°$ towards zero. Note that $C_1=0$ for $\varphi_p=0,\pi/2$.

Figure 13(b) displays the angular dependence of the increment $\Gamma_{[\overline{1}11]}$ calculated from Eq. (75). This dependence is not much different from the one predicted by Eq. (76). The angular distribution here has the form of a main lobe, situated in quadrant III, and a secondary one lying in quadrant IV.

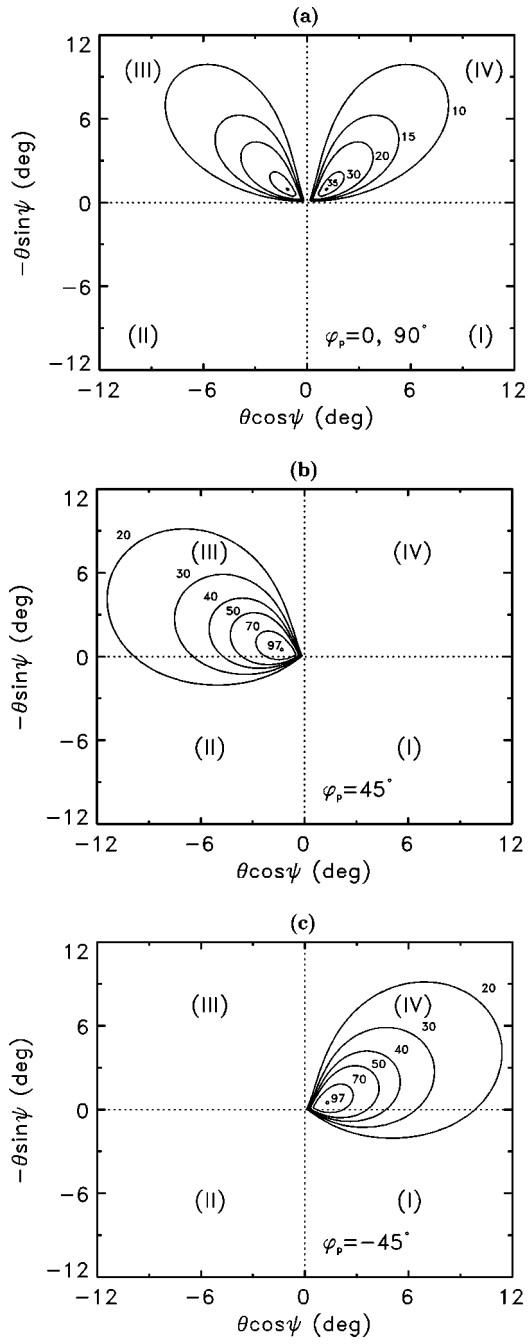

FIG. 12. Contour lines $\Gamma(\lambda\vec{K}/2\pi)=\mathrm{const}>0$ for the transversal configuration; the cases (a), (b), and (c) correspond to $\varphi_p=0,\pi/2$; $\varphi_p=\pi/4$; and $\varphi_p=-\pi/4$, respectively.

Now we turn to the diagonal configuration $\vec{E}_0 \| [111]$. In this case we should put $\zeta=\psi+\zeta_0$, $\varphi_2=\varphi_p+\zeta_0$ with $\zeta_0=-\arctan(\sqrt{2})\simeq-54.7°$. Using Eq. (65) and the symmetry properties of the functions $\nu_{0,1,3}$ mentioned in Sec. III, one easily finds that $\Gamma_{[111]}(\psi,\varphi_p,\theta)=\Gamma_{[\overline{1}11]}(-\psi,\varphi_p,\theta)$. In other words, the angular distributions of the increment for $[\overline{1}11]$ and [111] configurations transform into each other by a 180° rotation around the horizontal axis. In particular, by making this transformation, one can easily get from Fig. 13

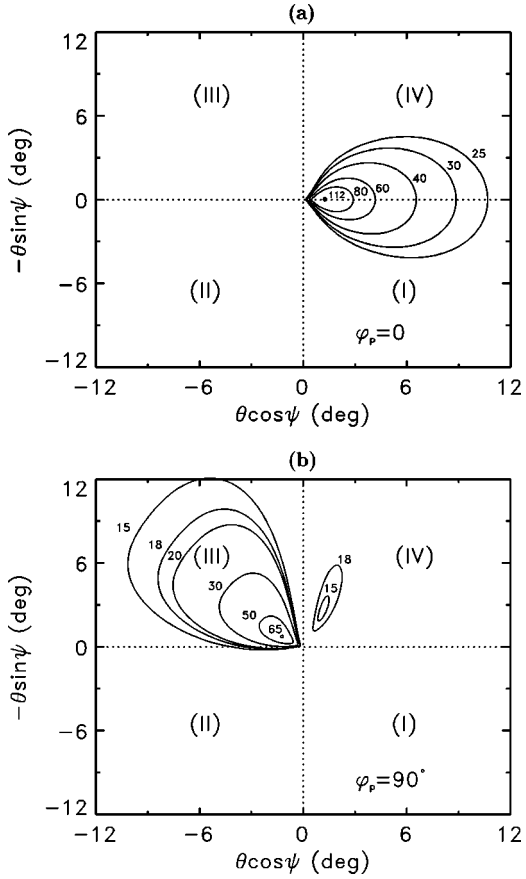

FIG. 13. Contour lines $\Gamma(\lambda\vec{K}/2\pi)=\text{const}>0$ for the diagonal configuration $[\overline{1}11]$; the cases (a) and (b) correspond to $\varphi_p=0$ and $\varphi_p=\pi/2$.

the angular distributions of $\Gamma_{[111]}(\psi,\theta)$ for $\varphi_p=0$ and $\pm\pi/2$. In accordance with the statements in Sec. III, the angular distributions for $\Gamma_{[\overline{1}11]}$ and $\Gamma_{[111]}$ look similar but they are not equivalent.

Finally, we consider the angular dependence of the increment for the backward configuration obtained from the diagonal $[\overline{1}11]$ configuration by a 180° rotation around the vertical axis [see Fig. 4(b)]. For this backward configuration we have $\zeta_0=\pi-\arctan(\sqrt{2})$ and another choice of the experimental variables ψ and φ_p: $\zeta=\psi+\pi-\arctan(\sqrt{2})$, $\varphi_2=\varphi_p+\pi-\arctan(\sqrt{2})$. The problem is to find the relationship between the increment $\Gamma_B(\psi,\varphi_p)$ for the backward geometry and the increment $\Gamma(\psi,\varphi_p)$ for the initial forward configuration. Using Eq. (63), the definition of $\nu_0,\vec{\nu},\vec{\kappa}$, and the properties of symmetry given by Eqs. (22), we easily obtain

$$\Gamma_B(\psi,\varphi_p,\theta)=-\Gamma(-\psi,-\varphi_p,\theta). \tag{77}$$

In what follows from the above relation, the dependences $\Gamma_B(\psi,\theta)$ for $\varphi_p=0,\pi/2$ may be obtained from the corresponding dependences $\Gamma(\psi,\theta)$ [see Figs. 13(a) and 13(b) by a 180° rotation around the vertical axis. The same relation (77) connects the increments for the initial [111] configuration and the corresponding backward one.

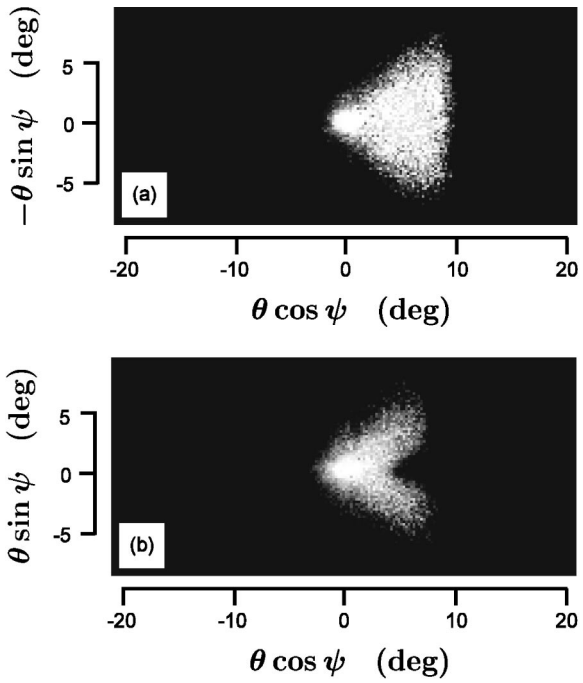

FIG. 14. Light-induced scattering in the longitudinal optical configuration. The patterns (a) and (b) correspond to the vertical and horizontal pump polarization, respectively.

IX. COMPARISON WITH EXPERIMENT

To compare the results of the previous section with experiment, we carried out measurements of light scattering patterns in BTO crystals for the longitudinal, transversal, and diagonal configurations. The experimental setup was similar to the one described in Refs. [10,30]. A laser beam of a wavelength $\lambda=632.8$ nm and a diameter $\simeq 1.2$ mm was incident normally onto the sample. The corresponding 2D distribution of scattered light was recorded in the far field with a CCD camera. Typical pump intensity and ac frequency were $\simeq 0.8$ W/cm^2 and 50 Hz, respectively. The amplitude of the square-wave ac field, $|E_0|$, ranged from 10 to 20 kV/cm. The moderate values of $|E_0|$ stem from the dimensions of the BTO samples used: $4\times5.9\times25.3$,$4.3\times2.5\times25.9$, and $3.3\times4.3\times9.9$ mm^3 for *L*, *T*, and *D* configurations, respectively. The first numbers are the interelectrode distances and the last ones are the crystal thicknesses, *l*. Unfortunately, samples with $l=4-7$ mm and with the interelectrode distance of $2-3$ mm, which seem to be the best for fanning experiments, were not available for us.

Figures 14(a) and 14(b) show the scattering patterns obtained in the longitudinal configuration ($\vec{E}_0\|[001]$) for the polarization angle $\varphi_p=90°$ and $\varphi_p=0$, respectively. These distributions have to be considered in conjunction with Figs. 11(a) and 11(b) for the increment $\Gamma(\theta,\psi)$. In agreement with theory, we have a one-lobe structure for the first and a two-lobe structure for the second case. Orientations of the lobes also meet the theoretical predictions. Note that the far right parts of the scattering lobes in Fig. 14 are cut by the crystal edge.

The light patterns presented in Fig. 15 are observed for the transversal configuration, $\vec{E}_0\perp[001]$. Two similar two-lobe patterns (a) and (b) correspond to the polarization angle

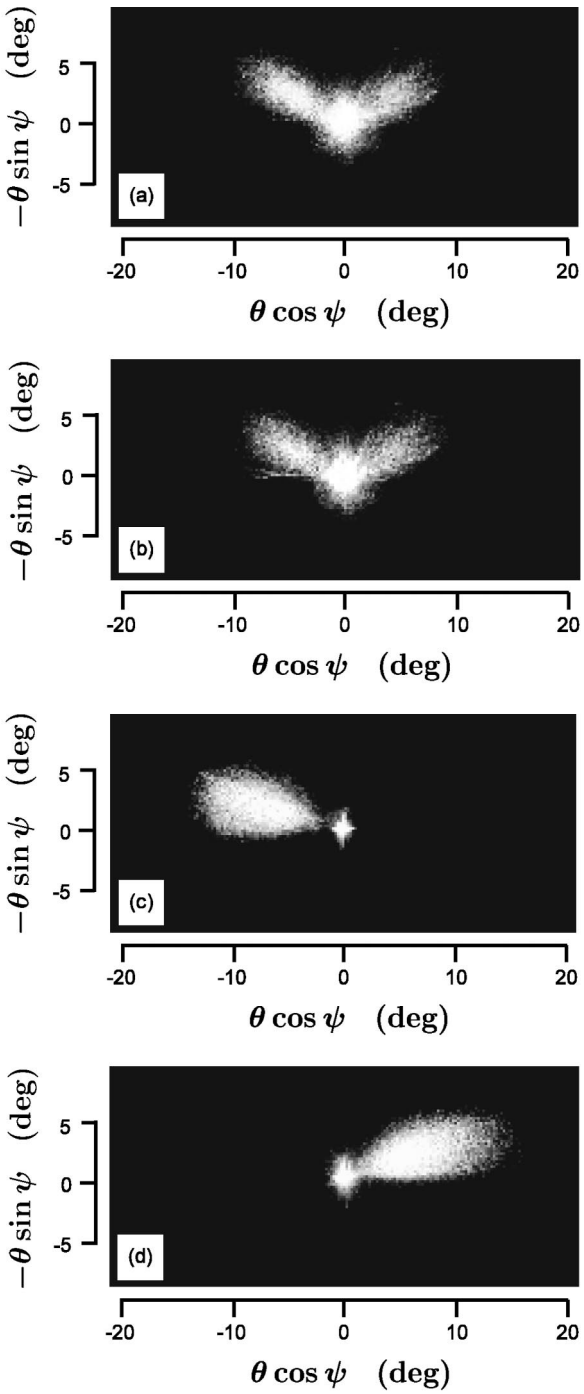

FIG. 15. Scattering patterns for the transversal optical configuration. The cases (a), (b), (c), and (d) correspond to the pump polarization angle φ_p equal 0°, 90°, 45°, and −45° to the horizontal.

$\varphi_p = 0$ and $\varphi_p = 90°$, respectively. They are in good qualitative agreement with the angular dependence of the increment given by Fig. 12(a). For $\varphi_p = 45°$ and $\varphi_p = -45°$ experiment gives one-lobe distribution of scattered light [see Figs. 15(c) and 15(d)]. Again, this is in harmony with the angular distribution of Γ shown in Figs. 12(b) and 12(c).

Last, Fig. 16 shows three different scattering patterns for the diagonal configuration, $\vec{E}_0 \| [\overline{111}]$. The strongest scattering is observed for the horizontal polarization, $\varphi_p = 0$ [see Fig. 16(a)]. In accordance with the theoretical Fig. 13(a), we have here one lobe of scattered light pointing at the horizontal direction $\psi_p = 0$. Switching the pump polarization from horizontal ($\varphi_p = 0$) to vertical ($\varphi = 90°$) dramatically changes the scattering pattern [see Fig. 16(b)]. The only lobe here points in the direction $\psi \simeq 220°$, which corresponds to the angular dependence of the increment given by Fig. 13(b). The light distribution of Fig. 16(c) is obtained for $\varphi_p = 90°$ after a 180° rotation of the sample around the vertical axis. In accordance with theory, it is not really different from the distribution obtained by a 180° rotation of Fig. 16(b) around the vertical.

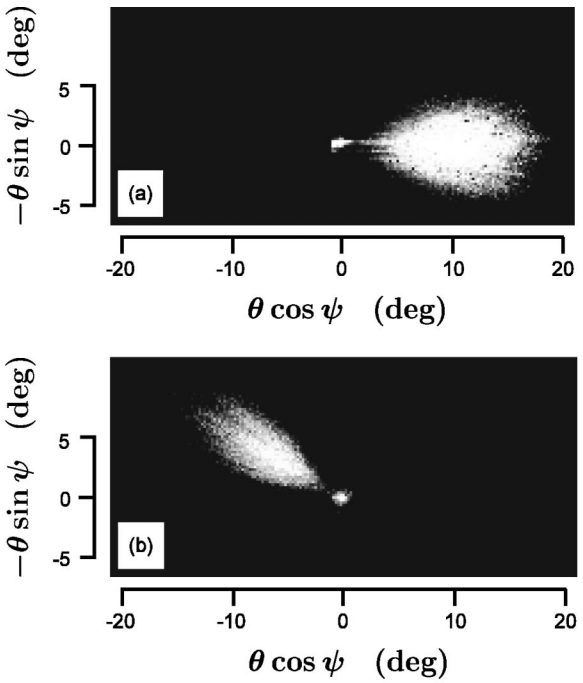

FIG. 16. Scattering distributions for the diagonal optical configuration $\vec{E}_0 \| [\overline{111}]$. Patterns (a) and (b) are obtained for $\varphi_p = 0$ and $\varphi_p = 90°$; pattern (c) is also obtained for the vertical polarization ($\varphi_p = 90°$), but the sample has been rotated prior by 180° around the vertical axis.

A clear feature of the light distributions shown in Figs. 15 and 16 is the separation of the scattering lobe(s) from the pump spot. This is especially pronounced for the cases of strong scattering [see Figs. 15(c) and 15(d) and 16(a)–16(c)], when the role of distortions of the pump spot is diminished. This feature is in line with theory which predicts decreasing scattering for sufficiently small scattering angles.

One more obvious point of qualitative agreement between theory and experiment is the polarization dependence of the scattering intensity for each of the above configurations. This agreement may be established by comparing the effect of light polarization on the brightness of the lobes and the effect of the same polarization on the value of the increment Γ (see Figs. 11–16).

Therefore, we have found good qualitative agreement between the main theoretical predictions for BTO crystals and experiment. A more detailed quantitative comparison between the theory and the observations is beyond the scope of this paper.

X. DISCUSSION

Let us summarize and discuss first the main merits of the analytical approach used as compared with the methods of

the preceding theoretical considerations. The developed theory is distinguished by a high level of generality. It covers a large variety of optical configurations relevant to experiment, it incorporates flexibly the accumulated results on the elasto-optic contributions to the photorefractive response, it includes the effects of optical activity and field-induced birefringence, and last, it allows one to describe the effect of enhancement of the space-charge field.

In spite of its generality, the theory remains fairly simple in form. Its main relations are highly informative but not unwieldy. Such a compromise is due to the extensive use of the properties of spatial symmetry, the use of a number of phenomenological characteristics known from experiments, and the introduction of the formalism of Pauli matrices.

The factors of different physical meaning are well separated in the theoretical expressions. Such a block structure makes the theory flexible and adjustable to the use of pieces of information extracted from different sources. For example, the angular dependence of the increment Γ is defined by the product of the enhancement factor $Q(\theta,\psi)$ (which is relevant to the known effects of excitation of space-charge waves [42]) and an azimuth factor dependent on the choice of the optical configuration and on the pump polarization. Realization of this fact allows one to connect the characteristics of different phenomena, to see the physical limitations on the light contrast, and to optimize the conditions for wave coupling.

The analytical expressions are highly useful for the introduction of various approximations: the undepleted pump approximations, the approximation of weak and strong optical activity, etc. An extensive analysis of particular and limiting cases is beyond the scope of this paper. We can indicate, however, some promising directions for application and generalization of the obtained results.

(i) Analysis of the rate of spatial amplification in the presence of a large dc field does not present any serious difficulties. It is of interest in view of early [47] and recent [48] experiments with BSO crystals.

(ii) The results obtained in Sec. VII within the undepleted pump approximation can easily be generalized to the case of circular and elliptic input polarizations. It is remarkable that the exponential amplification here can be free of the spatial oscillations.

(iii) The rate of spatial amplification Γ can be optimized with respect to the pump polarization and orientation of the applied ac field for an arbitrary value of the rotatory power, which is important for BSO and BGO crystals.

(iv) The effect of nonexponential spatial amplification, pronounced in BSO crystals, may be investigated in detail.

(v) The effect of wave coupling on the subharmonic generation in BSO and BTO crystals is worthy of a special study. This effect is clearly seen in ac experiments [49].

(vi) Vectorial four-wave processes of the phase conjugation and of the parametric scattering, as well as the surface wave formation in fiberlike BTO crystals, are also a challenge for the analytical theory.

XI. CONCLUSIONS

An analytical theory of the photorefractive vectorial wave coupling is developed for cubic crystals of the point group 23 and $\bar{4}3m$. In a unified manner the theory incorporates the effects of optical activity and field-induced birefringence, the influence of optoelasticity, and the enhancement of the photorefractive response by an ac field. It is applicable to a wide range of optical configurations and light polarizations, and adjustable to the introduction of various approximations. Applications of the theory are given to the analysis of the polarization and orientation characteristics of 2W coupling in BTO crystals. A good qualitative agreement with experimental data for BTO crystals is demonstrated. The prospects for further development and application of the obtained results are discussed.

ACKNOWLEDGMENTS

Financial support from INTAS and SFB 225 is gratefully acknowledged.

[1] *Photorefractive Materials and Their Applications, I and II*, edited by P. Günter and J.-P. Huignard, Topics in Applied Physics Vols. 61 and 62 (Springer-Verlag, Berlin, 1988 and 1989).

[2] M.P. Petrov, S.I. Stepanov, and A.V. Khomenko, *Photorefractive Crystals in Coherent Systems* (Springer-Verlag, Berlin, 1991).

[3] L. Solymar, D.J. Webb, and A. Grunnet-Jepsen, *The Physics and Applications of Photorefractive Materials* (Clarendon Press, Oxford, 1996).

[4] P. Refregier, L. Solymar, H. Rajbenbach, and J.-P. Huignard, J. Appl. Phys. **58**, 45 (1985).

[5] S.I. Stepanov and M.P. Petrov, Opt. Commun. **53**, 292 (1985).

[6] C.S.K. Walsh, A.K. Powell, and T.J. Hall, J. Opt. Soc. Am. B **7**, 288 (1990).

[7] A.A. Kamshilin, T. Jaaskelainen, C.J. Lima, M.R.B. Andreeta, and V.V. Prokofiev, Opt. Lett. **18**, 690 (1993).

[8] A.A. Kamshilin, R. Ravattinen, H. Tuovinen, T. Jaaskelainen, and V. Prokofiev, Opt. Commun. **103**, 221 (1993).

[9] E. Raita, A.A. Kamshilin, V.V. Prokofiev, and T. Jaaskelainen, Appl. Phys. Lett. **70**, 1641 (1997).

[10] A.A. Kamshilin, E. Raita, and A.V. Khomenko, J. Opt. Soc. Am. B **13**, 2536 (1996).

[11] A.A. Kamshilin, E. Raita, and T. Jaaskelainen, Opt. Rev. **3**, 443 (1996).

[12] E. Shamonina, K.H. Ringhofer, B.I. Sturman, G. Cedilnik, A. Kießling, R. Kowarschik, A.A. Kamshilin, V.V. Prokofiev, and T. Jaaskelainen, Opt. Lett. **23**, 1435 (1998).

[13] A. Marrakchi, R.V. Johnson, and A.R. Tanguay, J. Opt. Soc. Am. B **3**, 321 (1986).

[14] S. Mallick, D. Rouède, and A.G. Apostolidis, J. Opt. Soc. Am. B **4**, 1247 (1987).

[15] A. Brignon and K.H. Wagner, Opt. Commun. **101**, 239 (1993).

[16] B.I. Sturman, D.J. Webb, R. Kowarschik, E. Shamonina, and

K.H. Ringhofer, J. Opt. Soc. Am. B **11**, 1813 (1994).
[17] J.R. Goff, J. Opt. Soc. Am. B **12**, 99 (1995).
[18] N.V. Kukhtarev, G.E. Dovgalenko, and V.N. Starkov, Appl. Phys. A: Solids Surf. **33**, 227 (1984).
[19] S. Mallick and D. Rouède, Appl. Phys. B: Photophys. Laser Chem. **43**, 239 (1987).
[20] E. Shamonina, V.P. Kamenov, K.H. Ringhofer, G. Cedilnik, A. Kießling, and R. Kowarschik, J. Opt. Soc. Am. B **15** (to be published).
[21] J. Kumar, G. Albanese, and W.H. Steier, J. Opt. Soc. Am. B **4**, 1079 (1987).
[22] I. Auberecht, H.C. Ellin, A. Grunnet-Jepsen, and L. Solymar, J. Opt. Soc. Am. B **12**, 1918 (1995).
[23] A.A. Izvanov, A.E. Mandel, N.D. Khatkov, and A.E. Shandarovr, Optoelectron. Instrum. Data Process. **2**, 80 (1986).
[24] S. Stepanov, S.M. Shandarov, and N.D. Khat'kov, Phys. Solid State **29**, 1754 (1987).
[25] V.V. Shepelevich, S.M. Shandarov, and A.E. Mandel, Ferroelectrics **110**, 235 (1990).
[26] G. Pauliat, P. Mathey, and G. Roosen, J. Opt. Soc. Am. B **8**, 1942 (1991).
[27] V.V. Shepelevich, N.N. Egorov, and V. Shepelevich, J. Opt. Soc. Am. B **11**, 1394 (1994).
[28] S.M. Shandarov, A. Emelyanov, O. Kobozev, A. Reshet'ko, V.V. Volkov, and Yu.F. Kargin, Proc. SPIE **2801**, 221 (1996).
[29] M. Zgonik, K. Nakagava, and P. Günter, J. Opt. Soc. Am. B **12**, 1416 (1995).
[30] H. Tuovinen, A.A. Kamshilin, R. Ravattinen, V. Prokofiev, and T. Jaaskelainen, Opt. Eng. (Bellingham) **34**, 2641 (1995).
[31] H.C. Pedersen and P.M. Johansen, J. Opt. Soc. Am. B **12**, 592 (1996).
[32] H. Tuovinen, A.A. Kamshilin, and J. Jaaskelainen, J. Opt. Soc. Am. B **14**, 3383 (1997).
[33] P. Yeh, J. Opt. Soc. Am. B **4**, 1382 (1987).
[34] P. Yeh, IEEE J. Quantum Electron. **25**, 484 (1989).
[35] L.D. Landau and E.M. Lifshiz, *Quantum Mechanics* (Pergamon Press, Oxford, 1969).
[36] E. Merzbacher, *Quantum Mechanics* (Wiley, New York, 1970), Chap. 12, p. 271.
[37] L.D. Landau and E.M. Lifshiz, *Statistical Physics* (Pergamon Press, Oxford, 1969).
[38] J.F. Nye, *Physical Properties of Crystals* (Pergamon Press, Oxford, 1969).
[39] L.D. Landau and E.M. Lifshiz, *Field Theory* (Pergamon Press, Oxford, 1969).
[40] A. Yariv and P. Yeh, *Optical Waves in Crystals* (Wiley, New York, 1984).
[41] M. Born and E. Wolf, *Principles of Optics* (Pergamon, Oxford, 1959).
[42] B.I. Sturman, M. Mann, J. Otten, and K.H. Ringhofer, J. Opt. Soc. Am. B **10**, 1919 (1993).
[43] J. Takacs and L. Solymar, Opt. Lett. **17**, 247 (1992).
[44] G.A. Brost, J. Opt. Soc. Am. B **9**, 1454 (1992).
[45] M. Cronin-Golomb, B. Fisher, J.O. White, and A. Yariv, IEEE J. Quantum Electron. **20**, 12 (1984).
[46] H.C. Pedersen, D.J. Webb, and P.M. Johansen, J. Opt. Soc. Am. B **15**, 5 (1998).
[47] J.P. Herriau, D. Rojas, J.P. Huignard, J.M. Bassat, and J.C. Launau, Ferroelectrics **75**, 271 (1987).
[48] H.C. Ellin and L. Solymar, Opt. Commun. **130**, 85 (1996).
[49] H.C. Pedersen, P.M. Johansen, and D.J. Webb, J. Opt. Soc. Am. **15**, 2573 (1998).